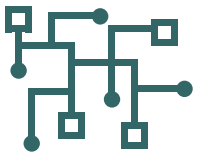

ISE

Industrial and Systems Engineering

Mixed-integer Second-order Cone Optimization for Composite Discrete Ply-angle and Thickness Topology Optimization Problems

Sicheng He, John T. Hwang, and Joaquim R. R. A. Martins

Dept. of Aerospace Engineering
University of Michigan, Ann Arbor, MI, USA

Mohammad Shahabsafa, Ali Mohammad-Nezhad, Weiming Lei, Luis Zuluaga, and Tamás Terlaky

Dept. of Industrial and Systems Engineering
Lehigh University, Bethlehm, PA, USA

ISE Technical Report 19T-014

LEHIGH UNIVERSITY

Mixed-integer Second-order Cone Optimization for Composite Discrete Ply-angle and Thickness Topology Optimization Problems

Sicheng He · Mohammad Shahabsafa · Weiming Lei · Ali Mohammad-Nezhad · Tamás Terlaky · Luis Zuluaga · Joaquim R. R. A. Martins ·

Abstract Discrete variable topology optimization problems are usually solved approximately by solid isotropic material with penalization (SIMP) type methods and genetic algorithms. In this paper, we propose reformulations of the discrete ply-angle and thickness topology optimization problems as a mixed-integer second-order cone optimization (MISOCO) problem. This differs from SIMP type methods and genetic algorithms in that a global optimal solution is guaranteed. We consider two types of problems: a mass minimization problem with the objective of saving mass from the structure, and a compliance optimization problem with the objective of making the structure as stiff as possible. For each element, besides whether material is present or not in the structure, we choose ply-angle and thickness from a finite set of possibilities. The discrete design space for ply-angle and thickness is a result of the manufacturing limitations. We also develop valid inequality constraints to tighten the continuous relaxation of the MISOCO reformulation and a warm start strategy effective for the mass minimization problem. We compare the performance of various MISOCO solvers: Gurobi, CPLEX, and MOSEK to solve the MISOCO reformulation. Based on this comparison, we recommend MOSEK for its efficiency.

Sicheng He, E-mail: hschsc@umich.edu
Joaquim R. R. A. Martins

Aerospace Engineering, University of Michigan,
Franois-Xavier Bagnoud Aerospace Building, 1320 Beal Avenue, Ann Arbor, MI 48109-2140

Mohammad Shahabsafa,
Weiming Lei,
Ali Mohammad-Nezhad,
Tamás Terlaky, E-mail: terlaky@lehigh.edu
Luis Zuluaga, E-mail: luz212@lehigh.edu

Department of Industrial and Systems Engineering,
Harold S. Mohler Laboratory, Lehigh University,
200 West Packer Avenue, Bethlehem, PA 18015-1582, USA

Keywords Laminated composites · Discrete ply-angle · Topology optimization · Global optimization · Branch-and-cut (B&C) · mixed-integer second-order conic optimization (MISOCO)

1 Introduction

The laminated composite optimization problem with ply-angle as a design variable is a classic structural optimization problem. In this problem, a structural performance metric, such as compliance or mass, is optimized with respect to the ply-angle in the laminated plate. This problem is classified into two categories with different types of design variables: (1) A continuous optimization problem in which the ply-angle is a continuous variable; (2) A mixed-integer optimization problem in which the ply-angle is picked from a discrete set. Ghiasi et al (2010) and Nikbakt et al (2018) provide more details on these types of problems.

The continuous ply-angle problem arises when using advanced manufacturing technology enabled by automated fiber placement machines (Brooks and Martins, 2018). A high-fidelity aerostructural optimization problem with continuous ply-angle variation has been formulated and applied to a aircraft wing design optimization problem by Brooks and Martins (2018). In other recent work, Zhou et al (2018) studied a multicomponent structures optimization problem and Brampton et al (2015) used a level set approach to solve the optimal ply-angle problem.

Discrete ply-angle composite structures are more economical to manufacture compared to the tow-steered composite structures. Thus, we focus on the discrete ply-angle optimization problem in this research. The discrete ply-angle optimization problem can be categorized as a discrete optimization problem that imposes additional challenges on both mathematical and numerical aspects. The main solution methods for the discrete ply-angle optimization problem is categorized into three classes: (1) Solid isotropic material with penalization (SIMP) type methods (Bendsøe and Sigmund, 1999); (2) Genetic algorithms (GA) and other gradient-free heuristics (Riche and Haftka, 1993); (3) Mixed-integer nonlinear optimization methods, especially mixed-integer convex optimization methods (MICO) (Grossmann et al, 1992; Stolpe and Svanberg, 2003)). We review each of these categories in more detail below.

SIMP type of methods encode the design variables into binary numbers. The continuous relaxation of the original mixed-integer problem is solved and a penalization is imposed on any fractional solution. As an enhanced SIMP type method, discrete material optimization (DMO) was proposed by Stegmann and Lund (2005) for discrete ply-angle optimization problem. Kennedy and Martins (2013) and Bruyneel (2010) provide alternative methods to DMO. The DMO technique has also been extended to include discrete thickness variables in Sørensen and Stolpe (2015). Recently, Kennedy (2016) proposed an interior point method to solve large-scale instances of the DMO formulations of the discrete ply-angle problem. However, these methods do not provide any guarantee that the solution obtained is globally optimal. In addition, SIMP type methods are usually presented without any benchmark cases comparing the SIMP results with known global optimal results.

GA methods have the advantage of being able to work directly with integer variables. Riche and Haftka (1993) apply a GA to the maximization of the buckling load with respect to the composite element stacking sequence. Kim et al (1999) presents a GA approach that minimizes the composite mass with a finite-element method (FEM) model. Gillet et al (2009) propose single and multi-objective optimization formulations with yield stress constraints. Albanesi et al (2018) combine a GA with inverse FEM with a maximum stress constraint. Nikbakt et al (2018) provides more details on the application of GA methods to composite optimization problems. They stated that "The convergency rate of these methods (GA) is lower than local search problems while the chance of obtaining the global optima is higher." Thus, similarly to SIMP type methods, there is no warranty that the solution obtained by GA methods is a global optimal solution. Another limitation of GA methods is that they lack the ability to handle large number of design variables due to the curse of dimensionality.

Similarly to GA methods, mixed-integer optimization also has the ability to handle integer variables directly. Researchers have converted different types of structural optimization problems into MILO, MISOCO, or general MICO formulations. The literature that is most related to the current research are the works of Munoz (2010) and Marmaras (2014). Using technique of Petersen (1971) (see Section 3), Munoz (2010) considers stress- and strain-constrained discrete ply-angle compliance and mass minimization problems. However, only the maximum strain constrained compliance optimization problem is solved and reported. The fact that the problem is not a topology optimization problem makes it less challenging compared to problems considered in current research. Marmaras (2014) presents a basic maximum stress constraint but does not show any test cases for the mass minimization problem.

The reformulation technique of Petersen (1971) has been used earlier to solve truss optimization problems as well. Grossmann et al (1992) and Stolpe and Svanberg (2003) reformulated the discrete truss size optimization problems as a mixed-integer linear optimization (MILO) problem. Several facets of this reformulations have been explored (Stolpe, 2007; Stolpe and Stidsen, 2007; Rasmussen and Stolpe, 2008; Achtziger and Stolpe, 2007; Stolpe, 2014). Mela (2014) extends this method to include buckling constraints for truss topology optimization and Shahabsafa et al (2018) propose a neighborhood search method to approximately solve the MILO problem with more than 12000 binary variables (Shahabsafa, 2018).

There are also other efforts that are not based on the technique by Petersen (1971). Haftka and Walsh (1992) formulate the buckling load optimization problem in which the aim is to find an optimal stacking sequence as a MILO problem. The MILO problem is solved with a branch-and-bound (B&B) algorithm. Recently, Sørensen and Lund (2015) solve the laminate composite compliance minimization problem to global optimality but without any local stress constraints.

In this work, we propose a MISOCO formulation to optimize composite structural mass or compliance in which the aim is to find optimal discrete ply-angles and discrete plate thicknesses. The second-order cone (SOC) constraint in the MISOCO formulation arises from the quadratic Tsai–Wu failure criterion (Hahn and Tsai, 1980). The approach leverages the efficient interior point algorithms developed for the underlying SOCO (second-order cone optimization) which is a continuous relaxation of the original problem (Andersen et al, 2003). Commercial solver developers

are currently working on solving large-scale MISOCO problems. Since the solution speed of MISOCO may vary a lot among different solvers, we also benchmark their performance. In this work, we consider three widely-used commercial optimization solvers: Gurobi (Gurobi Optimization, LLC, 2018), CPLEX (IBM ILOG, 2018), and MOSEK (Andersen and Andersen, 2000).

MISOCO problems are solved by branch-and-cut (B&C) methods. The efficiency of B&C methods is closely related to the tightness of the continuous relaxation problem. Recently, Belotti et al (2017) proposed the use of disjunctive conic cuts (DCC) for MISOCO problems to tighten the continuous relaxation of a MISOCO and in turn, speed up its solution. In the present work, we observe that the convex hull of the feasible disjunctive sets can be described using SOCs, inspired by the work of Belotti et al (2017). Based on this observation, we derive two valid conic inequalities to tighten the continuous relaxation of the original MISOCO problem. Also, when solving the MISOCO problem, if a feasible solution is found early with lower objective function, it can greatly reduce the computation time because many branches with higher objective function values could be ignored without wasting time exploring them. Thus, in commercial solvers, a portion of the computational time is used by heuristic methods that search for feasible solutions. Here, we explore the possibility of using a feasible solution found by other solver to warm start the MISOCO solver to reduce the computational cost.

In topology optimization problems, there is a well-known issue called stress singularity, which occurs when the stress constraints remain active while no material is present in an element. This may cause a feasible solution to be misclassified as an infeasible one. This issue was first reported by Sved and Ginos (1968) and later addressed by Cheng (1995) and Cheng and Guo (1997) with a technique called ε-relaxation. However, the stress singularity is not an issue in our proposed methodology because if material is not selected for a certain element, the corresponding stress with that material selection is automatically set to zero, which satisfies the stress constraint.

The checkerboard patterned solutions are an issue in topology optimization where the solution exhibits alternate solid and void elements. This issue is believed to be caused by an inadequate numerical modeling of the structure stiffness (Diaz and Sigmund, 1995; Sigmund, 1998). Filtering methods have been developed to prevent the checkerboard pattern issue (Sigmund, 1994; Bourdin, 2001). This involves averaging the solution in a neighborhood. In this paper, we show that the checkerboard pattern can be prevented by adding a set of linear constraints to the problem's MISOCO reformulation.

The paper is organized as follows. In Section 2, we describe the problem and formulate it as a mixed-integer nonlinear optimization (MINLO). We describe the Petersen (1971) method that is later used to reformulate the problem as a MISOCO in Section 3. We discuss four formulations for the quadratic Tsai–Wu failure criterion in Section 4. In Section 5, we discuss the method used to scale the problem, which has a positive impact on the numerical performance of optimization algorithms. In Section 6, we present numerical results. Finally, we present our conclusions in Section 7.

2 Problem formulation

In this section, we briefly introduce all the components involved in the structural optimization problems of interest and their mathematical formulations.

2.1 Structural mass

The total mass of the structure is:

$$W = \sum_{i=1}^{N} \sum_{j=1}^{M} z_{ij} w_{ij}, \tag{1}$$

where W is the total mass, w_{ij} is the mass of i^{th} element with j^{th} option chosen and z_{ij} is the binary choice variable—$z_{ij} = 1$ if j^{th} option is used and $z_{ij} = 0$ otherwise. In total we have N elements, $i \in \{1, 2, \ldots, N\}$ and M options, which could include potential discrete ply-angle choices, discrete thickness choices, or both, $j \in \{1, 2, \ldots, M\}$. Since we do not consider different materials in this research, the mass is proportional to volume, so it is fully determined by the i^{th} element geometry. Therefore, we can remove the common density factor and set $w_{ij} = l_{i,x} l_{i,y} h_j$. Here, $l_{i,x}, l_{i,y}$ are the length in the x and y directions, and h_j is the j^{th} discrete thickness option. For optimization problems without thickness variables, the uniform value h_j could be dropped from the mass in equation (1).

2.2 Compliance

Compliance measures how much energy is stored in the structure under a given external load. A stiffer structure stores less energy compared to a softer one under the same load. The mathematical expression for the compliance is given by

$$C = \mathbf{f}_{\text{ext}}^{\mathsf{T}} \mathbf{u}, \tag{2}$$

where C is the compliance, $\mathbf{f}_{\text{ext}} \in \mathbb{R}^n$ is the external load, $\mathbf{u} \in \mathbb{R}^n$ is the structural displacement, and n denotes the FEM degree-of-freedom. The function is linear since the external load $\mathbf{f}_{\text{ext}}$ is a constant vector.

2.3 Finite-element Method

Since we apply a simultaneous analysis and design (SAND) approach (Haftka, 1985; Martins and Lambe, 2013), the FEM model of the structure also appears as problem constraints that are directly handled by the optimizer itself. When using a FEM, a global stiffness matrix $\mathbf{K}$ is formed and the displacement vector $\mathbf{u}$ is computed by solving the linear system

$$\mathbf{K}\mathbf{u} = \mathbf{f}_{\text{ext}}, \tag{3}$$

where $\mathbf{K} \in \mathbb{R}^{n \times n}$. But $\mathbf{K} = \mathbf{K}(z_{1,1}, \ldots, z_{N,M})$ need to take all the design variables as parameters and we may also encounter reduction of the degree-of-freedom due

to the appearance of void elements in the topology optimization problem. Instead, Stolpe and Svanberg (2003) found that it is easier to manipulate the local equilibrium equation, which is only dependent on local design variables. Following Stolpe and Svanberg (2003), we decompose the global equilibrium equation into many smaller pieces. In Section 3 we also show how to reformulate all the bilinear terms in these equations using linear inequality constraints.

For each plate element, we have the local equilibrium equation to relate the local displacement to the local internal load:

$$\begin{aligned}&\mathbf{f}_i = \mathbf{K}_i \mathbf{u}_i,\\ &\mathbf{K}_i = \sum_{j=1}^{M} z_{ij}\mathbf{K}_{ij}, \forall i \in \{1,\ldots,N\},\end{aligned}$$

where $\mathbf{f}_i \in \mathbb{R}^{n_{\text{elem}}}$ is the internal load for the i^{th} element (n_{elem} is the number of degrees-of-freedom per element), $\mathbf{u}_i \in \mathbb{R}^{n_{\text{elem}}}$ denotes the local displacement in the i^{th} element, $\mathbf{K}_i \in \mathbb{R}^{n_{\text{elem}} \times n_{\text{elem}}}$ is the local stiffness matrix, and $\mathbf{K}_{ij} = \mathbf{K}_{ij}(\theta_j, h_j)$ is the local stiffness matrix corresponding with j^{th} discrete variable option.

The external loads are balanced by the internal loads at node s as follows,

$$\sum_{i \in \delta(s)} \mathbf{H}_i^s \mathbf{f}_i + \mathbf{f}_{\text{ext}}^s = 0, \forall s \in \mathbf{S} - \mathbf{S}_{\text{bdr}}.$$

where $\delta(s)$ is the set of elements that contains s, $\mathbf{H}_i^s \in \mathbb{R}^{n_{\text{elem}} \times n_{\text{node}}}$ is a matrix mapping to the load at s (n_{node} is number of degrees-of-freedom per node), $\mathbf{f}_{\text{ext}}^s \in \mathbb{R}^{n_{\text{node}}}$ is the external load at s, $\mathbf{S}$ is the set of FEM model nodes, and $\mathbf{S}_{\text{bdr}}$ is the set of boundary nodes.

We consider the clamped boundary condition, meaning that there are no translational or rotational displacements at the boundary, i.e.,

$$\mathbf{u}^s = 0, \forall s \in \mathbf{S}_{\text{bdr}},$$

where $\mathbf{u}^s$ denotes the displacement at node s.

2.4 Local stress constraints

In a feasible design, the stress should be within the yield bounds. In this section, we present the formulation of the stress constraints and the equations linking stresses, strains, and displacement.

The strain is a dimensionless variable that characterizes how much the structure is deformed and is fully determined by the displacement field. For a plate element, the strain can be written as

$$\begin{aligned}&\varepsilon_i^l = \sum_j \varepsilon_{ij}^l,\\ &\varepsilon_{ij}^l = z_{ij}\mathbf{B}_{ij}(\mathbf{x}_{ij}^l)\mathbf{u}_i,\ \forall i \in \{1,\ldots,N\},\end{aligned} \tag{4}$$

where $\boldsymbol{\varepsilon}_i^l \in \mathbb{R}^3$ is the in-plane strain in the i^{th} element at node l with coordinate $\mathbf{x}_{ij}^l \in \mathbb{R}^3$, $\boldsymbol{\varepsilon}_{ij}^l \in \mathbb{R}^3$ is the strain at the monitored point if the j^{th} option is picked; $\mathbf{B}_{ij}(\mathbf{x}_{ij}^l) \in \mathbb{R}^{n_{\text{elem}} \times 3}$ is a matrix that is determined by the local coordinates $\mathbf{x}_{ij}^l$ and also the element thickness. In this study, we choose to monitor the strain at the center point on the upper surface of a plate element: $\mathbf{x}_{ij}^l = \left(\mathbf{x}_{ij,c}, \mathbf{y}_{ij,c}, \frac{h_j}{2}\right)^\intercal$ where h_j is the j^{th} option plate thickness, where $\mathbf{x}_{ij,c}$ and $\mathbf{y}_{ij,c}$ denote the $\mathbf{x}$ and $\mathbf{y}$ coordinates of the center point from i^{th} element.

The stress is a measure of how much the structure is loaded locally and is dependent on the strain field through the relation

$$\boldsymbol{\sigma}_{ij}^l = \mathbf{Q}_j \boldsymbol{\varepsilon}_{ij}^l, \tag{5}$$

where $\boldsymbol{\sigma}_{ij}^l \in \mathbb{R}^3$ is the in-plane stress when the j^{th} option is picked for the i^{th} element at l, and the constitutive matrix $\mathbf{Q}_j \in \mathbb{R}^{3\times 3}$ is detailed in the appendix.

When an excessive load is applied to the structure, the structure yields. This must be avoided in any engineering design. The yield constraint is formulated using the Tsai–Wu failure criterion for composite structures (Tsai and Wu, 1971)

$$\bar{\boldsymbol{\sigma}}_{ij}^{l\,\intercal} \bar{\mathbf{P}} \bar{\boldsymbol{\sigma}}_{ij}^l + 2\bar{\mathbf{q}}^\intercal \bar{\boldsymbol{\sigma}}_{ij}^l - 1 \leq 0, \tag{6}$$

where

$$\bar{\mathbf{P}} = \begin{bmatrix} \frac{1}{X_t|X_c|} & -\frac{1}{2}\frac{1}{\sqrt{X_t X_c Y_t Y_c}} & 0 \\ -\frac{1}{2}\frac{1}{\sqrt{X_t X_c Y_t Y_c}} & \frac{1}{Y_t|Y_c|} & 0 \\ 0 & 0 & \frac{1}{S^2} \end{bmatrix}, \bar{\mathbf{q}} = \frac{1}{2}\begin{bmatrix} \frac{1}{X_t} - \frac{1}{|X_c|} \\ \frac{1}{Y_t} - \frac{1}{|Y_c|} \\ 0 \end{bmatrix}. \tag{7}$$

Here, $\bar{\boldsymbol{\sigma}}_{ij}^l$ is the in-plane stress in the i^{th} element for the j^{th} option at l in the fiber coordinates and "$\bar{\cdot}$" denotes variables expressed in the coordinate aligned with the fiber orientation. Also, $\bar{\mathbf{P}}$ and $\bar{\mathbf{q}}$ are dependent on the material selection. Since we do not consider multiple materials, $\bar{\mathbf{P}}$ and $\bar{\mathbf{q}}$ are constant matrices. Parameters X_c and X_t are the composite tension and compression failure strengths for the direction parallel to the fiber direction, respectively. Parameters Y_c and Y_t are the tension and compression failure strengths in the direction perpendicular to the fiber orientation. Finally, parameter S is the shear strength. Note that $X_c < 0$, $Y_c < 0$, $X_t > 0$, $Y_t > 0$, $S > 0$ and are constant numbers, since we consider single composite material. Thus, $\bar{\mathbf{P}}$ is positive definite. To express this in local x, y coordinates, we need to conduct a transformation operation $\bar{\boldsymbol{\sigma}}_{ij}^l = \mathbf{T}_j(\theta_j)\boldsymbol{\sigma}_{ij}^l$ (The details about the $\mathbf{T}_j$ matrix are given in Appendix 1). Thus, we have

$$\boldsymbol{\sigma}_{ij}^{l\,\intercal}\left(\mathbf{T}_j^\intercal \bar{\mathbf{P}} \mathbf{T}_j\right)\boldsymbol{\sigma}_{ij}^l + 2\left(\bar{\mathbf{q}}^\intercal \mathbf{T}_j\right)\boldsymbol{\sigma}_{ij}^l - 1 \leq 0. \tag{8}$$

For simplicity, we define the following notation

$$\mathbf{P}_j \coloneqq \mathbf{T}_j^\intercal \bar{\mathbf{P}} \mathbf{T}_j, \mathbf{q}_j \coloneqq \mathbf{T}_j^\intercal \bar{\mathbf{q}}.$$

In addition, the yield constraint should only be enforced when j^{th} design is actually chosen, i.e., $z_{ij} = 1$. Otherwise, the constraint should not come into effect. This has already been taken into account in equation (4)—when $z_{ij} = 0$, we have $\boldsymbol{\varepsilon}_{ij}^l = 0$.

Consequently, according to equation (5), $\sigma_{ij} = 0$ and equation (8) is satisfied. Finally we have,

$$\begin{aligned}
&\varepsilon_{ij}^{l} = z_{ij}\mathbf{B}_{ij}(\mathbf{x}_{ij}^{l})\mathbf{u}_i, \\
&\varepsilon_{ij}^{l\,\mathsf{T}}\left(\mathbf{Q}_j^{\mathsf{T}}\mathbf{P}_j\mathbf{Q}_j\right)\varepsilon_{ij}^{l} + 2\mathbf{q}_j^{\mathsf{T}}\mathbf{Q}_j\varepsilon_{ij}^{l} - 1 \leq 0, \forall i \in \{1,\ldots,N\}, \forall j \in \{1,\ldots,M\}.
\end{aligned}$$

We reformulate this equation later in our proposed MISOCO formulations.

2.5 Logic constraints

For topology optimization, we could have either some material present at a candidate element or no material, which can be expressed as

$$\begin{aligned}
&z_i = \sum_j z_{ij}, \\
&z_i \leq 1,\ \forall i \in \{1,\ldots,N\},
\end{aligned}$$

where z_i denotes whether any material is present at the i^{th} element—if $z_i = 0$, then there is no material present; otherwise, if $z_i = 1$, some material is present.

2.6 Manufacturing constraints

Here we consider the manufacturing-related constraint for the composite material. We enforce the adjacency constraint: the neighboring element shall not have a change of ply-angle more than 45°. With a discrete design space where the angle options are

$$\{0, 45^\circ, 90^\circ, 135^\circ\}, \tag{9}$$

which are encoded in $z_{i,1}, z_{i,2}, z_{i,3}$ and $z_{i,4}$. This restriction is enforced by the following constraints

$$\begin{aligned}
&z_{i,1} + z_{p,3} \leq 1, \\
&z_{i,2} + z_{p,4} \leq 1, p \in \mathbf{N}(i),\ \forall i \in \{1,\ldots,N\},
\end{aligned} \tag{10}$$

where $\mathbf{N}(i)$ denotes the neighboring elements indices set of the i^{th} element. Later, in the numerical tests, this constraint is considered for problem in which the ply-angle choices are given by equation (9). When the choices for the angle are limited to $\{0^\circ, 90^\circ\}$, this constraint is not considered.

2.7 Checkerboard constraints

We enforce constraints to avoid the previously mentioned checkerboard pattern issue, which is illustrated in Figure 1.

The constraint is based on the observation that when the checkerboard pattern is present, the sum of the binary design variables is 2 on one diagonal and 0 on the other diagonal, and the absolute difference of the sums is 2. Otherwise, the difference

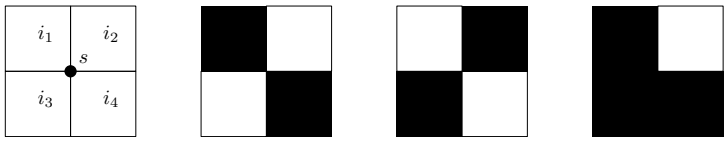

Fig. 1: Checkerboard illustration. The first figure shows the element indexing where s is an interior point of the FEM model and i_1, i_2, i_3 and i_4 are the neighboring element indices; the second and third figures exhibit a checkerboard pattern; while the last one does not. For the second and third figures, we have $|(z_{i_1} + z_{i_3}) - (z_{i_2} + z_{i_4})| = 2$ and for the last one $|(z_{i_1} + z_{i_3}) - (z_{i_2} + z_{i_4})| = 1$, so it satisfies equation (11).

is either be 0 or 1. By setting the difference less or equal to 1, results with the checkerboard pattern are eliminated from the feasible set. The mathematical formulation is:

$$-1 \leq (z_{i_1} + z_{i_3}) - (z_{i_2} + z_{i_4}) \leq 1,\ (i_1, i_2, i_3, i_4) = \mathbf{N}_{\text{nbr}}(s), \forall s \in \mathbf{S}_{\text{int}}, \qquad (11)$$

where $\mathbf{N}_{\text{nbr}}(s)$ are the set of neighboring elements of node s. And s is any point from the set of interior points, $\mathbf{S}_{\text{int}}$, (i.e., points with four neighboring elements) in the FEM model. This is a novel formulation to restrict the checkerboard pattern.

2.8 MINLO formulation

In this section, we present the mass minimization and compliance minimization problems with discrete ply-angle and discrete thickness variables.

2.8.1 Stress-constrained mass minimization problem

Using the results from Sections 2.1 to 2.7, we formulate the following MINLO problem

(MINLO-w)

$$\begin{aligned}
\min_{\mathbf{u}_i, \mathbf{f}_i, z_{ij}, z_i, \boldsymbol{\varepsilon}^l_{ij}} \quad & \sum_{i=1}^{N} \sum_{j=1}^{M} z_{ij} w_{ij} & \\
\text{s.t.} \quad & \mathbf{f}_i = \left(\sum_{j=1}^{M} z_{ij} \mathbf{K}_{ij} \right) \mathbf{u}_i & \forall i \in \{1, \ldots, N\} \\
& \sum_{i \in \delta(s)} \mathbf{H}_i^s \mathbf{f}_i + \mathbf{f}_{\text{ext}}^s = 0 & \forall s \in \mathbf{S} - \mathbf{S}_{\text{bdr}} \\
& \mathbf{u}^s = 0 & \forall s \in \mathbf{S}_{\text{bdr}} \\
& \boldsymbol{\varepsilon}^l_{ij} = z_{ij} \mathbf{B}_{ij}(\mathbf{x}^l_{ij}) \mathbf{u}_i & \forall i \in \{1, \ldots, N\}, \forall j \in \{1, \ldots, M\} \\
& \boldsymbol{\varepsilon}^{l\,\intercal}_{ij} \left(\mathbf{Q}_j^\intercal \mathbf{P}_j \mathbf{Q}_j \right) \boldsymbol{\varepsilon}^l_{ij} + 2 \mathbf{q}_j^\intercal \mathbf{Q}_j \boldsymbol{\varepsilon}^l_{ij} - 1 \leq 0 & \forall i \in \{1, \ldots, N\}, \forall j \in \{1, \ldots, M\} \\
& z_i = \sum_{j=1}^{M} z_{ij} & \forall i \in \{1, \ldots, N\} \\
& z_i \leq 1 & \forall i \in \{1, \ldots, N\} \\
& -1 \leq (z_{i_1} + z_{i_3}) - (z_{i_2} + z_{i_4}) \leq 1 & (i_1, i_2, i_3, i_4) = \mathbf{N}_{\text{nbr}}(s), \forall s \in \mathbf{S}_{\text{int}} \\
& z_{ij} \in \{0, 1\} & \forall i \in \{1, \ldots, N\}, \forall j \in \{1, \ldots, M\}.
\end{aligned}$$

Recall that the manufacturing constraints equation (10) are enforced when the design variable set contains four options as given in equation (9). Otherwise, for example, if the choices of the ply-angle are limited to $\{0, 90^\circ\}$, we drop this constraint.

2.8.2 Stress-constrained compliance minimization problem

The compliance optimization problem is similar to the mass minimization problem (MINLO-w), so it shares most of its constraints. The differences are: (1) The objective function is the compliance (2) instead of mass (1)); (2) One additional constraint is added as the mass upper bound, which is expressed as

$$\sum_{i=1}^{N}\sum_{j}^{M} z_{ij} w_{ij} \leq W_{\max}$$

where $W_{\max}$ is the upper bound of structural mass. For brevity, we only discuss the mass optimization problem formulations, but all the results apply in similar fashion to the compliance minimization problem.

The continuous relaxation of the original problem for both the mass and compliance optimization problems is nonconvex due to several bilinear terms involving the z_{ij} and $\mathbf{u}_i$ design variables. In Section 3, we show how to linearize these constraints so that the problem can be reformulated as a MISOCO, that is, a problem whose underlying continuous relaxation problem is a SOCO problem. Unlike MINLO problems, MISOCO problems can be solved to global optimality.

3 MISOCO reformulation

To address the nonconvexity of the bilinear equality constraint in (MINLO-w), we apply the method of Petersen (1971), where the equality constraints involving products of binary variables and continuous variables can be reformulated as a set of linear constraints. We replace $z_{ij}\mathbf{u}_i$ with ψ_{ij} where $\mathbf{L}$ and $\mathbf{U}$ are lower and upper bounds on $\mathbf{u}_i$ to obtain

$$\psi_{ij} = z_{ij}\mathbf{u}_i, \mathbf{L} \leq \mathbf{u}_i \leq \mathbf{U}. \tag{12}$$

If the bounds $\mathbf{L}$ and $\mathbf{U}$ are given, we can use them directly. Otherwise, we must estimate $\mathbf{L}$ and $\mathbf{U}$. In practice, we can make an empirical estimate by constructing a structure filled with material and then computing the absolute value of the displacement as $|\mathbf{u}_{i,F}|$. We then set $\mathbf{L}(k) = -\gamma \max_i |\mathbf{u}_{i,\mathbf{f}_{\text{ext}}}(k)|, \mathbf{U}(k) = \gamma \max_i |\mathbf{u}_{i,\mathbf{f}_{\text{ext}}}(k)|$, where $\gamma \geq 1$ is a parameter set by the user (we set $\gamma = 10$ by trail and error).

Equation (12) is equivalent with the following inequalities

$$\begin{cases} z_{ij}\mathbf{L} \leq \psi_{ij} \leq z_{ij}\mathbf{U} \\ (z_{ij}-1)\mathbf{U} + \mathbf{u}_i \leq \psi_{ij} \leq (z_{ij}-1)\mathbf{L} + \mathbf{u}_i \end{cases}, \tag{13}$$

where ψ_{ij} is the "pseudo displacement", which is the same as the "true displacement" $\mathbf{u}_i$ if the material j is picked; otherwise, it is set to zero. With this reformulation, the

nonlinear and nonconvex equality constraints in (MINLP-w) are converted to linear inequalities.

The Petersen method is illustrated in Figure 2. The intuition we gain from this figure is that we can use the convex hull (green) of the original manifold (red) to substitute the original manifold itself. The convex hull turns out to be a polyhedron. Note that equation (13) is equivalent to the McCormick cuts associated with equation (12).

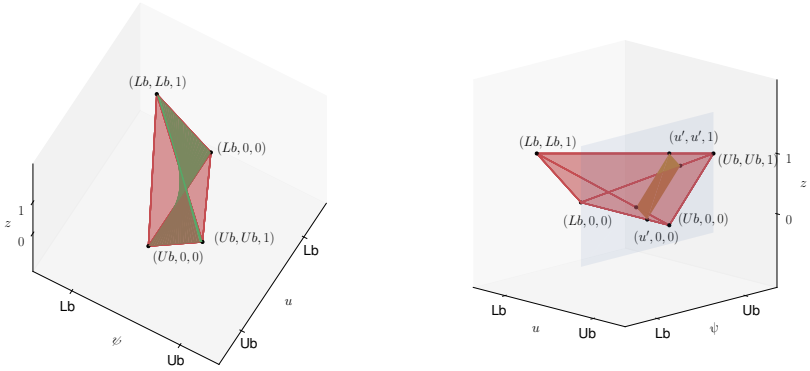

(a) (b)

Fig. 2: Visualization of the Petersen method. On the left: the original nonconvex set (green) formed by $\{(u,\psi,z) : \psi = zu, z \in [0,1], L \le u \le U\}$ and the convex hull (red) $\{(u,\psi,z) : zL \le \psi \le zU, (z-1)U+u \le \psi \le (z-1)L+u, z \in [0,1], L \le u \le U\}$. On the right: the convex hull (red) intersected with a plane (blue): $\{(u,\psi,z) : u = u'\}$ and the intersection area (brown).

4 Tsai–Wu failure criterion formulations

In this section, we present four alternative formulations for the Tsai–Wu constraints. Two out of the four formulations are based on a SOC tightening.

4.1 MISOCO reformulation with smaller dimensional ellipsoidal constraints

We refer to the stress constraint in (MINLO-w) as a small ellipsoid constraint (Tsai–Wu-se), since the quadratic term defines an ellipsoid ($\mathbf{Q}_j^\mathsf{T}\mathbf{P}_j\mathbf{Q}_j$ is positive-definite) and the constraints are decoupled among different designs (i.e ε_{ij_1} and $\varepsilon_{ij_2}, j_1 \neq j_2$ are decoupled in the constraints). This constraint is given as

(Tsai–Wu-se): $\varepsilon_{ij}^{l\,\mathsf{T}} \left(\mathbf{Q}_j^\mathsf{T}\mathbf{P}_j\mathbf{Q}_j\right) \varepsilon_{ij}^{l} + 2\mathbf{q}_j^\mathsf{T}\mathbf{Q}_j\varepsilon_{ij}^{l} - 1 \le 0, \forall i \in \{1,\ldots,N\}, \forall j \in \{1,\ldots,M\},$

which is a special SOC constraint, the so-called rotated cone constraint (Andersen et al, 2003).

Applying the Peterson method (13) to (MINLO-w), we get a MISOCO formulation that we name it (MISOCO-se),

(MISOCO-se)

$$
\begin{aligned}
\min_{\mathbf{u}_i,\mathbf{f}_i,z_{ij},z_i,\boldsymbol{\varepsilon}^l_{ij}} \quad & \sum_{i=1}^{N}\sum_{j=1}^{M} z_{ij} w_{ij} & \\
\text{s.t.} \quad & z_{ij}\mathbf{L} \le \boldsymbol{\psi}_{ij} \le z_{ij}\mathbf{U} & \forall i \in \{1,\dots,N\}, \forall j \in \{1,\dots,M\} \\
& (z_{ij}-1)\mathbf{U} + \mathbf{u}_i \le \boldsymbol{\psi}_{ij} \le (z_{ij}-1)\mathbf{L} + \mathbf{u}_i & \forall i \in \{1,\dots,N\}, \forall j \in \{1,\dots,M\} \\
& \mathbf{f}_i = \sum_{j=1}^{M} \mathbf{K}_{ij}\boldsymbol{\psi}_{ij} & \forall i \in \{1,\dots,N\} \\
& \sum_{i\in\delta(s)} \mathbf{H}_i^s \mathbf{f}_i + \mathbf{f}_{\text{ext}}^s = 0 & \forall s \in \mathbf{S} - \mathbf{S}_{\text{bdr}} \\
& \mathbf{u}^s = 0 & \forall s \in \mathbf{S}_{\text{bdr}} \\
& \boldsymbol{\varepsilon}^l_{ij} = \mathbf{B}_{ij}(\mathbf{x}^l_{ij})\boldsymbol{\psi}_{ij} & \forall i \in \{1,\dots,N\}, \forall j \in \{1,\dots,M\} \\
& \boldsymbol{\varepsilon}^{l\,\intercal}_{ij} \left(\mathbf{Q}_j^\intercal \mathbf{P}_j \mathbf{Q}_j\right) \boldsymbol{\varepsilon}^l_{ij} + 2\mathbf{q}_j^\intercal \mathbf{Q}_j \boldsymbol{\varepsilon}^l_{ij} - 1 \le 0 & \forall i \in \{1,\dots,N\}, \forall j \in \{1,\dots,M\} \\
& z_i = \sum_{j=1}^{M} z_{ij} & \forall i \in \{1,\dots,N\} \\
& z_i \le 1 & \forall i \in \{1,\dots,N\} \\
& -1 \le (z_{i_1} + z_{i_3}) - (z_{i_2} + z_{i_4}) \le 1 & (i_1,i_2,i_3,i_4) = \mathbf{N}_{\text{nbr}}(s), \forall s \in \mathbf{S}_{\text{int}} \\
& z_{ij} \in \{0,1\} & \forall i \in \{1,\dots,N\}, \forall j \in \{1,\dots,M\}.
\end{aligned}
$$

In the (MISOCO-se) formulation, we have $N \times M$ binary design variables, z_{ij}. The intermediate variable z_i is of dimension N and can be avoided during implementation. As for continuous variables, we have $N_{\text{DOF per element}} \times N \times M$ continuous variable, $\boldsymbol{\psi}_{ij}$ where $N_{\text{DOF per element}}$ indicates the degree-of-freedom per element; $3 \times N \times M$ continuous variable, $\boldsymbol{\varepsilon}^l_{ij}$, where the number 3 is the dimension of in plane strain; $N_{\text{DOF per element}} \times N$ variables for $\mathbf{f}_i$; and $N_{\text{total DOF}}$ for $\mathbf{u}_i$ where $N_{\text{total DOF}}$ is the total degree-of-freedom of the FEM model. To sum it up, the number of continuous variables is of the order of $N_{\text{DOF per element}} \times N \times M$. The linear constraints can be easily counted from the formulation. For the SOCO constraints, we have a total of $N \times M$ SOCO constraints with three variables for each one of them.

4.2 MISOCO reformulation with larger dimensional ellipsoidal constraints (MISOCO–le)

An alternative Tsai–Wu failure criterion formulation is

$$
\mathbf{u}_i^\intercal \left(\sum_j z_{ij} \mathbf{B}_{ij}(\mathbf{x}^l_{ij})^\intercal (\mathbf{x}^l_{ij}) \mathbf{Q}_j^\intercal \mathbf{P}_j \mathbf{Q}_j \mathbf{B}_{ij}(\mathbf{x}^l_{ij}) \right) \mathbf{u}_i + 2 \sum_j \left(z_{ij} \mathbf{q}_j^\intercal \mathbf{Q}_j \mathbf{B}_{ij}(\mathbf{x}^l_{ij}) \right) \mathbf{u}_i - 1 \le 0, \tag{14}
$$

which we explain below. When none of the choices are active ($z_i = 0$), this simplifies to $-1 \le 0$, which is valid. Otherwise, one of the choices, j^* is active, i.e, $z_{ij^*} = 1$ and

$z_{ij} = 0, \forall j \neq j^*$. According to equation (14), we have

$$\mathbf{u}_i^\intercal \mathbf{B}_{ij^*}^\intercal(\mathbf{x}_{ij^*}^l)\mathbf{Q}_{j^*}^\intercal \mathbf{P}_{j^*}\mathbf{Q}_{j^*}\mathbf{B}_{ij}(\mathbf{x}_{ij^*}^l)\mathbf{u}_i + 2\left(\mathbf{q}_{j^*}^\intercal \mathbf{Q}_{j^*}\mathbf{B}_{ij^*}(\mathbf{x}_{ij^*}^l)\right)\mathbf{u}_i - 1 \leq 0,$$

which is the Tsai–Wu failure criterion (8), together with the displacement-strain relationship (4), and stress-strain relationships (5), so we know it is also valid. However, the constraint is not a quadratic constraint, because the first term involves products of $\mathbf{u}_{ij}^\intercal$, z_{ij} and $\mathbf{u}_{ij}$.

Equation (14) can be converted to a quadratic constraint as follows (Munoz, 2010)

$$\begin{aligned}
& \sum_j \left((z_{ij}\mathbf{u}_i^\intercal)\left(\mathbf{B}_{ij}(\mathbf{x}_{ij}^l)^\intercal \mathbf{Q}_j^\intercal \mathbf{P}_j \mathbf{Q}_j \mathbf{B}_{ij}(\mathbf{x}_{ij}^l)\right)(z_{ij}\mathbf{u}_i)\right) + 2\sum_j \mathbf{q}_j^\intercal \mathbf{Q}_j \mathbf{B}_{ij}(\mathbf{x}_{ij}^l)(z_{ij}\mathbf{u}_i) - 1 \leq 0, \quad && \forall i \in \{1,\ldots,N\}, \\
\Leftrightarrow \quad & \sum_j \left(\boldsymbol{\psi}_{ij}^\intercal \left(\mathbf{B}_{ij}(\mathbf{x}_{ij}^l)^\intercal \mathbf{Q}_j^\intercal \mathbf{P}_j \mathbf{Q}_j \mathbf{B}_{ij}(\mathbf{x}_{ij}^l)\right)\boldsymbol{\psi}_{ij}\right) + 2\sum_j \mathbf{q}_j^\intercal \mathbf{Q}_j \mathbf{B}_{ij}(\mathbf{x}_{ij}^l)\boldsymbol{\psi}_{ij} - 1 \leq 0, && \forall i \in \{1,\ldots,N\}, \\
\Leftrightarrow \quad & \text{(Tsai–Wu-le): } \sum_j \left(\boldsymbol{\varepsilon}_{ij}^{l\,\intercal}\left(\mathbf{Q}_j^\intercal \mathbf{P}_j \mathbf{Q}_j\right)\boldsymbol{\varepsilon}_{ij}^l\right) + 2\sum_j \mathbf{q}_j^\intercal \mathbf{Q}_j \boldsymbol{\varepsilon}_{ij}^l - 1 \leq 0, && \forall i \in \{1,\ldots,N\}.
\end{aligned}$$

In the first step, we leverage on the fact that: $z_{ij}^2 = z_{ij}$ if $z_{ij} \in \{0,1\}$. In the second step, we use $z_{ij}\mathbf{u}_i = \boldsymbol{\psi}_{ij}$ implied by equation (13). And in the last step, we apply $\mathbf{B}_{ij}(\mathbf{x}_{ij}^l)\boldsymbol{\psi}_{ij} = \boldsymbol{\varepsilon}_{ij}$. Unlike (Tsai–Wu-le), this constraint couples $\boldsymbol{\varepsilon}_{ij_1}^l$ with $\boldsymbol{\varepsilon}_{ij_2}^l, \forall j_1 \neq j_2$. We refer to this as Tsai–Wu-le ("le" for large ellipsoid). However, this formulation also reduces the total number of SOCO constraints—in total, there are N constraints compared with $N \times M$ for (Tsai–Wu-se) constraints. If (Tsai–Wu-le) is used in (MISOCO–se) to substitute (Tsai–Wu-le), we name the optimization problem as (MISOCO–le).

4.3 SOC-based valid inequality reformulation

4.3.1 Valid inequality construction

In the previous Tsai–Wu yield constraint formulations, we consider $\boldsymbol{\varepsilon}_{ij}^l$ by itself. If we group $\boldsymbol{\varepsilon}_{ij}^l$ and z_{ij} and consider the corresponding Tsai–Wu failure criterion in equation (4) and (8), then the feasible domain, $(\boldsymbol{\varepsilon}_{ij}^l, z_{ij}) \in S_{\text{disj}}$, is

$$S_{\text{disj}} = \{(0,0)\} \cup \{(\boldsymbol{\varepsilon}_{ij}^l, 1) | \boldsymbol{\varepsilon}_{ij}^{l\,\intercal} \mathbf{Q}_j^\intercal \mathbf{P}_j \mathbf{Q}_j \boldsymbol{\varepsilon}_{ij}^l + 2\mathbf{q}_j^\intercal \mathbf{Q}_j \boldsymbol{\varepsilon}_{ij}^l - 1 \leq 0\}.$$

However, the (Tsai–Wu-se) by itself is a "loose" constraint whose feasible domain is $\{(\boldsymbol{\varepsilon}_{ij}^l, z_{ij})\} \in S_{\text{se}}$,

$$\begin{aligned}
S_{\text{se}} = & \{(\boldsymbol{\varepsilon}_{ij}^l, 0) | \boldsymbol{\varepsilon}_{ij}^{l\,\intercal} \mathbf{Q}_j^\intercal \mathbf{P}_j \mathbf{Q}_j \boldsymbol{\varepsilon}_{ij}^l + 2\mathbf{q}_j^\intercal \mathbf{Q}_j \boldsymbol{\varepsilon}_{ij}^l - 1 \leq 0\}\} \\
& \cup \{(\boldsymbol{\varepsilon}_{ij}^l, 1) | \boldsymbol{\varepsilon}_{ij}^{l\,\intercal} \mathbf{Q}_j^\intercal \mathbf{P}_j \mathbf{Q}_j \boldsymbol{\varepsilon}_{ij}^l + 2\mathbf{q}_j^\intercal \mathbf{Q}_j \boldsymbol{\varepsilon}_{ij}^l - 1 \leq 0\},
\end{aligned} \tag{15}$$

i.e., with $z_{ij} = 0$, the feasible domain for $\boldsymbol{\varepsilon}_{ij}^l$ is the same as with $z_{ij} = 1$ if we only consider the yield constraints.

To make the constraint tighter, we construct the convex hull of S_{disj}, which is given as

$$S_{\text{SOC}} = \left\{ (\boldsymbol{\varepsilon}_{ij}^l, z_{ij}) | \begin{bmatrix} \boldsymbol{\varepsilon}_{ij}^{l\,\intercal} & z_{ij} \end{bmatrix} \begin{bmatrix} \mathbf{Q}_j^\intercal \mathbf{P}_j \mathbf{Q}_j & \mathbf{Q}_j^\intercal \mathbf{q}_j \\ \mathbf{q}_j^\intercal \mathbf{Q}_j & -1 \end{bmatrix} \begin{bmatrix} \boldsymbol{\varepsilon}_{ij}^l \\ z_{ij} \end{bmatrix} \leq 0, z_{ij} \geq 0 \right\}. \tag{16}$$

The set S_{SOC} contains S_{disj}. On one hand, when $z_{ij} = 0$, we have $\boldsymbol{\varepsilon}_{ij}^l \in \{\boldsymbol{\varepsilon}_{ij}^l | \boldsymbol{\varepsilon}_{ij}^{l\,\intercal} \mathbf{Q}_j \mathbf{P}_j \mathbf{Q}_j \boldsymbol{\varepsilon}_{ij}^l \leq 0\}$. Since $\mathbf{Q}_j^\intercal \mathbf{P}_j \mathbf{Q}_j$ is positive definite, we have $\boldsymbol{\varepsilon}_{ij}^l \in \{0\}$. On the other hand, when $z_{ij}^l = 1$, it recovers to $\{(\boldsymbol{\varepsilon}_{ij}^l, 1) | \boldsymbol{\varepsilon}_{ij}^{l\,\intercal} \mathbf{Q}_j^\intercal \mathbf{P}_j \mathbf{Q}_j \boldsymbol{\varepsilon}_{ij}^l + 2\mathbf{q}_j^\intercal \mathbf{Q}_j \boldsymbol{\varepsilon}_{ij}^l - 1 \leq 0\}$.

All three sets, $S_{\text{disj}}, S_{\text{se}}, S_{\text{SOC}}$, are shown in Figure 3.

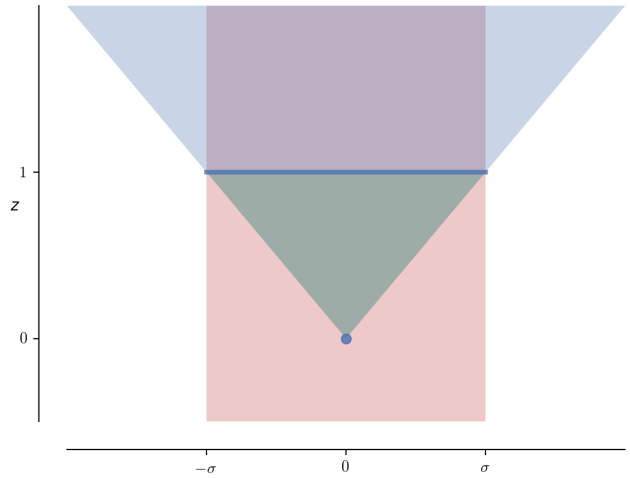

Fig. 3: S_{SOC} (blue shaded), $\text{Conv}(S_{\text{se}})$ the convex hull of Tsai–Wu-se constraint (red), $\text{Conv}(S_{\text{disj}})$ convex hull of feasible disjunctive sets (green) and S_{disj}, the original disjunctive set (blue solid).

Finally, we present a proof showing that the constraint derived is indeed a SOC:

Claim S_{SOC} defines a SOC.

Proof Following the convention by Belotti et al (2013), we define the set of points from equation (16) as

$$Q = \{\mathbf{w} | \mathbf{w}^\intercal \mathbf{P} \mathbf{w} + 2\mathbf{p}^\intercal \mathbf{w} + \rho \leq 0\}, \tag{17}$$

where

$$\begin{aligned} \mathbf{P} &= \begin{bmatrix} \mathbf{Q}_j^\intercal \mathbf{P}_j \mathbf{Q}_j & \mathbf{Q}_j^\intercal \mathbf{q}_j \\ \mathbf{q}_j^\intercal \mathbf{Q}_j & -1 \end{bmatrix}, \\ \mathbf{p} &= 0, \\ \rho &= 0. \end{aligned} \tag{18}$$

According to Belotti et al (2013), Q is a SOC if $\mathbf{P}$ has exactly one negative eigenvalue, is non-singular, and in addition the following condition is satisfied:

$$\mathbf{p}^\intercal \mathbf{P}^{-1} \mathbf{p} - \rho = 0. \tag{19}$$

By equation (18), $\mathbf{p} = 0$ and $\rho = 0$, so equation (19) is satisfied. Therefore, it suffices to show that $\mathbf{P}$ has only one negative eigenvalue and all other eigenvalues are positive. We decompose $\mathbf{P}$ into the product of three matrices

$$\begin{bmatrix} \mathbf{Q}_j^\intercal \mathbf{P}_j \mathbf{Q}_j & \mathbf{Q}_j^\intercal \mathbf{q}_j \\ \mathbf{q}_j^\intercal \mathbf{Q}_j & -1 \end{bmatrix} = \begin{bmatrix} I & \mathbf{Q}_j^\intercal \mathbf{q}_j \\ 0 & 1 \end{bmatrix}^{-1} \begin{bmatrix} \mathbf{Q}_j^\intercal \mathbf{P}_j \mathbf{Q}_j + \mathbf{Q}_j^\intercal \mathbf{q}_j \mathbf{q}_j^\intercal \mathbf{Q}_j & 0 \\ 0 & -1 \end{bmatrix} \begin{bmatrix} I & 0 \\ \mathbf{q}_j^\intercal \mathbf{Q}_j & 1 \end{bmatrix}^{-1}. \tag{20}$$

Now it suffices to show that the matrix in the middle of the RHS of equation (20) has three positive eigenvalues and one negative eigenvalue. Note that $\mathbf{Q}_j^\intercal \mathbf{P}_j \mathbf{Q}_j + \mathbf{Q}_j^\intercal \mathbf{q}_j \mathbf{q}_j^\intercal \mathbf{Q}_j$ is a sum of a positive definite (PD) matrix and a positive semi-definite (PSD) matrix (we prove $\mathbf{Q}_j^\intercal \mathbf{P}_j \mathbf{Q}_j$ PD later), so it is PD. We conduct an eigenvalue decomposition of $\mathbf{Q}_j^\intercal \mathbf{P}_j \mathbf{Q}_j + \mathbf{Q}_j^\intercal \mathbf{q}_j \mathbf{q}_j^\intercal \mathbf{Q}_j$:

$$\begin{bmatrix} \mathbf{Q}_j^\intercal \mathbf{P}_j \mathbf{Q}_j + \mathbf{Q}_j^\intercal \mathbf{q}_j \mathbf{q}_j^\intercal \mathbf{Q}_j & 0 \\ 0 & -1 \end{bmatrix} = \begin{bmatrix} \mathbf{V}_j & 0 \\ 0 & 1 \end{bmatrix} \begin{bmatrix} \boldsymbol{\Lambda}_j & 0 \\ 0 & -1 \end{bmatrix} \begin{bmatrix} \mathbf{V}_j^\intercal & 0 \\ 0 & 1 \end{bmatrix}, \tag{21}$$

where $\mathbf{V}_j$ and $\boldsymbol{\Lambda}_j$ are the eigenvector and eigenvalue of $\mathbf{Q}_j^\intercal \mathbf{P}_j \mathbf{Q}_j + \mathbf{Q}_j^\intercal \mathbf{q}_j \mathbf{q}_j^\intercal \mathbf{Q}_j$. Because $\mathbf{Q}_j^\intercal \mathbf{P}_j \mathbf{Q}_j + \mathbf{Q}_j^\intercal \mathbf{q}_j \mathbf{q}_j^\intercal \mathbf{Q}_j$ is PD, $\boldsymbol{\Lambda}_j > 0$. In addition, since the RHS of equation (21) is an eigenvalue decomposition of the LHS matrix, we conclude the LHS matrix has 3 positive eigenvalues and 1 negative eigenvalue of the LHS matrix.

Finally we show that $\mathbf{Q}_j^\intercal \mathbf{P}_j \mathbf{Q}_j$ is PD. We know $\mathbf{Q}_j$ is non-singular, so it suffices to show that $\mathbf{P}_j$ is PD. Because $\mathbf{P}_j = \mathbf{T}_j^\intercal \bar{\mathbf{P}} \mathbf{T}_j$, $\mathbf{T}_j$ is non-singular (it is a rotation matrix whose determinant is ± 1), it suffices to prove that $\bar{\mathbf{P}}$ is PD. Since $\bar{\mathbf{P}}$ is symmetric (refer to equation (7)), we only need to show that the leading principal minors of $\bar{\mathbf{P}}$ are all positive. The three leading principal minors are:

$$M_1 = \frac{1}{X_t |X_c|}, M_2 = \frac{3}{4 X_t X_c X_t X_c}, M_3 = \frac{3}{4 X_t X_c X_t X_c S^2}, \tag{22}$$

with $X_t > 0$, $Y_t > 0$, $X_t > 0$, $X_c < 0$, $S > 0$, we have $M_1, M_2, M_3 > 0$. This completes the proof. □

4.3.2 Sparse reformulation

The first inequality from equation (16) can be reformulated as

$$\begin{aligned} &{\varepsilon_{ij}^l}^\intercal \mathbf{Q}_j^\intercal \left(\mathbf{P}_j + \mathbf{q}_j \mathbf{q}_j^\intercal \right) \mathbf{Q}_j \varepsilon_{ij}^l \leq \left(-{\varepsilon_{ij}^l}^\intercal \mathbf{Q}_j^\intercal \mathbf{q}_j + z_{ij} \right)^2, \\ &-{\varepsilon_{ij}^l}^\intercal \mathbf{Q}_j^\intercal \mathbf{q}_j + z_{ij} \geq 0. \end{aligned} \tag{23}$$

There is an "alternative" cone with ${\varepsilon_{ij}^l}^\intercal \mathbf{Q}_j^\intercal \mathbf{q}_j - z_{ij} \geq 0$ that is not the cone we want. This is because the point $(\varepsilon_{ij}^l, z_{ij}) = (0,1)$, representing a design without any external load, which should be a feasible design, does not satisfy this inequality.

A detail about the SOC constraint (23) is that we can not directly use this form for the Gurobi MISOCO solver. Instead, we need to convert it to the appropriate form: $\mathbf{x}^\intercal\mathbf{x} \leq y^2, y \geq 0$. For that purpose, we conduct an eigenvalue decomposition for $\mathbf{Q}_j^\intercal\left(\mathbf{P}_j + \mathbf{q}_j\mathbf{q}_j^\intercal\right)\mathbf{Q}_j$:

$$\mathbf{Q}_j^\intercal\left(\mathbf{P}_j + \mathbf{q}_j\mathbf{q}_j^\intercal\right)\mathbf{Q}_j = \mathbf{V}_j\Lambda_j\mathbf{V}_j^\intercal,$$

where $\mathbf{V}_j$ and $\Lambda_j > 0$ are the eigenvector matrix and the eigenvalue matrix respectively. Then, we have:

$$\text{(Tsai–Wu-sparse SOC):} \begin{cases} \mathbf{x}_{ij}^\intercal\mathbf{x}_{ij} \leq y_{ij}^2, \\ y_{ij} \geq 0, \\ \mathbf{x}_{ij} = \sqrt{\Lambda_j}\mathbf{V}_j^\intercal\boldsymbol{\varepsilon}_{ij}^l, \\ y_{ij} = -\boldsymbol{\varepsilon}_{ij}^{l\intercal}\mathbf{Q}_j^\intercal\mathbf{q}_j + z_{ij}, \end{cases},$$

that is, a SOC constraint and two additional linear constraints. We refer to this as a "sparse SOC" because $\mathbf{x}_{ij}$ is only dependent on $\boldsymbol{\varepsilon}_{ij}$ in comparison with a dependence on both $\boldsymbol{\varepsilon}_{ij}$ and z_{ij} in (Tsai–Wu-dense SOC). We refer to the optimization problem with this specific constraint as (MISOCO–SOC-sparse).

4.3.3 Dense reformulation

Alternatively, we conduct the eigenvalue decomposition with the whole system in equation (16)

$$\begin{bmatrix} \mathbf{Q}_j^\intercal\mathbf{P}_j\mathbf{Q}_j & \mathbf{Q}_j^\intercal\mathbf{q}_j \\ \mathbf{q}_j^\intercal\mathbf{Q}_j & -1 \end{bmatrix} = \tilde{\mathbf{V}}_j \begin{bmatrix} \lambda_{neg,j} & 0 \\ 0 & \tilde{\boldsymbol{\Lambda}}_j \end{bmatrix} \tilde{\mathbf{V}}_j^\intercal, \lambda_{neg,j} < 0, \tilde{\boldsymbol{\Lambda}}_j > 0. \tag{24}$$

The conic constraint (24) is recast as:

$$\text{(Tsai–Wu-dense SOC):} \begin{cases} \mathbf{x}_{ij}^\intercal\mathbf{x}_{ij} \leq y_{ij}^2, \\ y_{ij} \geq 0, \\ \begin{bmatrix} y_{ij} \\ \mathbf{x}_{ij} \end{bmatrix} = \begin{bmatrix} \sqrt{-\lambda_{neg,j}} & 0 \\ 0 & \sqrt{\tilde{\boldsymbol{\Lambda}}_j} \end{bmatrix} \tilde{\mathbf{V}}_j^\intercal \begin{bmatrix} \varepsilon_{ij}^l \\ z_{ij} \end{bmatrix}. \end{cases}$$

As discussed in Section 4.3.2, $(\varepsilon_{ij}^l, z_{ij}) = (0,1)$ is a feasible point, we enforce that $\tilde{\mathbf{V}}_j[4,1] \geq 0$, instead of the other branch. We refer to the optimization problem with this specific constraint as (MISOCO–SOC-dense).

5 Scaling

The problem scaling is critical for numerical stability and the optimization solver performance. The goal is to bring the nonzero parameters close to the range of $[10^{-1}, 10]$ in absolute value. We use the scaling strategy of Kennedy (2016). Two parameters (α_m, α_s) are used to adjust the scaling for length and time scales. The scalings for the models are shown in Table 1.

The parameters α_m and α_s are selected based on the matrices entries range. In this work, we choose the parameter $\alpha_m = 10^{-6}, \alpha_s = 10^{-2}$, the corresponding matrix coefficients range is about $[10^{-3}, 10^4]$.

Table 1: Scaling of parameters from MISOCO formulations

Before scaling	After scaling
$\mathbf{K}_{ij}$	$\alpha_m \mathbf{K}_{ij}$
$\mathbf{f}_{\text{ext}}^s$	$\frac{\alpha_m}{\alpha_s} \mathbf{f}_{\text{ext}}^s$
$\mathbf{Q}_j^\mathsf{T} \mathbf{P}_j \mathbf{Q}_j$	$\alpha_s^2 \mathbf{Q}_j^\mathsf{T} \mathbf{P}_j \mathbf{Q}_j$
$\mathbf{Q}_j^\mathsf{T} \mathbf{q}_j$	$\alpha_s \mathbf{Q}_j^\mathsf{T} \mathbf{q}_j$
$\mathbf{U}, \mathbf{L}$	$\frac{1}{\alpha_s}\mathbf{U}, \frac{1}{\alpha_s}\mathbf{L}$

6 Results

In this section, we conduct numerical studies of the different stress formulations presented in Section 4 by using different commercial optimization packages. All the cases are run on a work station with 10 threads. For all cases in this section, we consider a cantilevered plate subject to a tip load, as shown in Figures 4a and 7a. The total length of each side is 1 m. The load is 4.2×10^5 N in the direction perpendicular to the paper surface at the right lower corner. We consider both 3×3 and 4×4 plates for each problem. The FEM element used in this research is a quadratic plate FEM model (which is similar to the one considered by Huang and Friedmann (2016), except that we drop nonlinear terms in the FEM model). Further details are given in Appendix 3. For each element, we have nine nodes and each node has three displacement and two rotation variables. The material properties are listed in Table 2.

Table 2: Carbon-epoxy material properties

Property	Value
E_{11}	146860 MPa
E_{22}	10620 MPa
ν_{12}	0.33
ν_{23}	0.33
G_{12}	5450 MPa
G_{23}	3990 MPa
X_t	1035 MPa
X_c	689 MPa
Y_t	41 MPa
Y_c	117 MPa
S_{12}	69 MPa

6.1 Stress constrained mass minimization problem

We consider a topology optimization problem where we minimize the mass of a cantilever plate subject to a tip load as shown in Figures 4a and 7a.

6.1.1 Discrete ply-angle variables only

The plate thickness is 0.1 m. The design variables are the orientation of each element that is restricted to be chosen either $0^\circ, 45^\circ, 90^\circ, 135^\circ$ or no material present.

For the 3×3 case, the solution time is given in Table 10 and the optimal solution is shown in Figure 4a. All solvers are able to get the optimal solution, but the speed to reach the solution is different. In three out of four formulations, CPLEX is faster than Gurobi and for only one formulation CPLEX is slower than Gurobi with a difference of 5%. MOSEK is the fastest for all formulations among the three solvers. Between solving the different formulations using MOSEK, the two with SOC introduced in Section 4.3, (MISOCO-SOC-sparse) and (MISOCO-SOC-dense), have a similar performance and are faster than the other two formulations, (MISOCO-le) and (MISOCO-se). The continuous relaxation solution times are similar among solvers and thus cannot explain the speed of MOSEK. A detailed convergence history is shown in Figure 5. For all solvers and all four formulations, fewer than 0.5% of the total nodes have been explored before optimality gap is closed. From Figure 5, we observe that MOSEK explores the least nodes among all solvers, which may explain its higher solution speed compared with the other two solvers. Also, compared to CPLEX, Gurobi explores more nodes for all cases, which explains its slower convergence speed for this case.

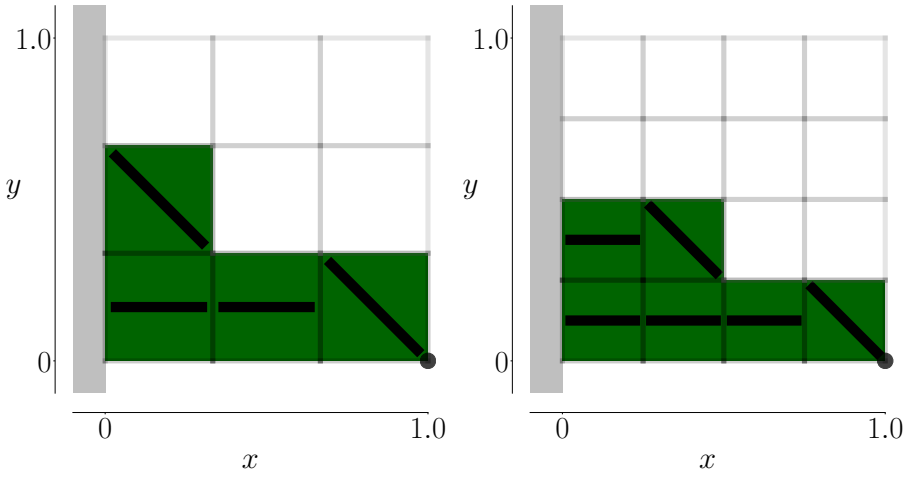

(a) 3×3 (b) 4×4

Fig. 4: Mass minimization result with discrete ply-angle variables. Both the 3×3 and 4×4 are solved to global optimality. The black lines indicate the ply orientation.

We use MOSEK to solve for the 4×4 case to global optimality and the result is shown in Figure 4b. About 0.00007% of all possible combinations have been ex-

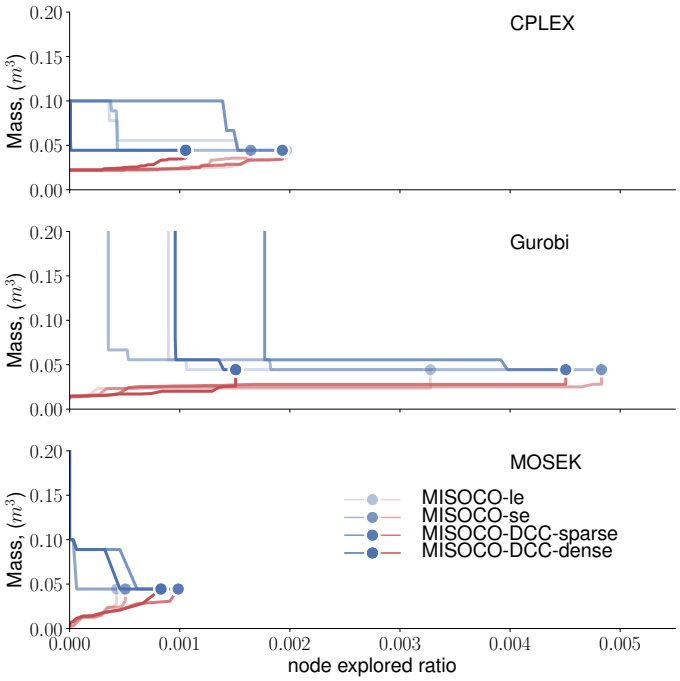

Fig. 5: Convergence history for different solvers using different formulations for the 3×3 discrete ply-angle only mass minimization problem. x axis is the ratio of nodes explored versus the total node numbers which is equal to $(M+1)^N = 5^9$. The y axes represent the mass (in m^3, after dropping constant density). The red and blue curves are the lower and upper bounds, respectively. The blue dots indicates the point where optimality gap has been closed.

Table 3: Discrete ply-angle mass minimization problem optimization time (sec) of different commercial solvers for 3×3 case

	Mixed integer optimization			Continuous relaxation		
	CPLEX	Gurobi	MOSEK	CPLEX	Gurobi	MOSEK
MISOCO–le	238.34	313.20	61.81	0.32	0.59	0.45
MISOCO–se	184.95	413.22	61.83	0.42	0.52	0.53
MISOCO–SOC-sparse	286.36	337.48	40.88	0.54	0.54	0.50
MISOCO–SOC-dense	159.53	151.86	41.65	0.58	0.59	0.57

plored for this case, even fewer than the 3×3 case. A detailed convergence history is shown in Figure 6.

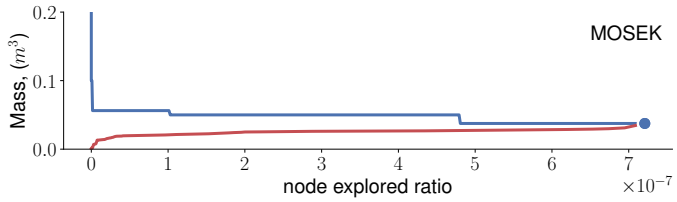

Fig. 6: Convergence history for MOSEK using MISOCO-se formulation for the 4×4 discrete ply-angle only mass minimization problem. The x axis is the ratio of nodes explored versus the total node numbers which is equal to $(M+1)^N = 5^{16}$. The y axis represents the mass (in m^3 after dropping constant density). The red and blue curves are the lower and upper bounds, respectively. The blue dot indicates the point where optimality gap has been closed.

Table 4: Discrete ply-angle mass minimization problem optimization time (sec) for 4×4 case using MOSEK

	Mixed integer optimization	Continuous relaxation
MISOCO–se	10521.35	1.00

6.1.2 Discrete ply-angle and discrete thickness variables

In this section, we add discrete thickness as a design variable to our problem. The thickness could be either 0.1 m or 0.03 m. We restrict the ply-angle options to $\{0^\circ, 90^\circ\}$ and drop the manufacturing constraint for this section, since it would otherwise forces all the plates to be orientated in the same direction.

For the 3×3 case, the optimal solution is shown in Figure 7a. All three optimizers are able to find this solution. We compare the solution times in Table 5. Contrary with what we found previously in Table 10 for the pure discrete ply-angle case, Gurobi outperforms CPLEX in the quadratic constraint case for three out of four cases. There is only one case in which CPLEX outperforms Gurobi, and for that case is within a margin of 10%.

Similarly to Table 10, MOSEK achieves the best solution time for all cases among the three solvers. For MOSEK, (MISOCO–le), (MISOCO–SOC-sparse), and (MISOCO–SOC-dense) results in a similar simulation time and is faster than (MISOCO–le). The continuous relaxation solution times are similar among solvers and thus cannot explain the fact that MOSEK is faster.

A detailed convergence history is shown in Figure 8. For all solvers solving all four formulations, fewer than 0.35% of total nodes were explored before the optimality gap was closed. We observe that MOSEK explore far less nodes compared with the other two solvers. Between Gurobi and CPLEX, the comparison of the number of nodes explored ratio explains its supremacy in terms of solution time— besides

the (MISOCO-se) formulation, Gurobi explores more nodes and takes more time to close the optimality gap; and for the (MISOCO-se) formulation, the reverse occurs.

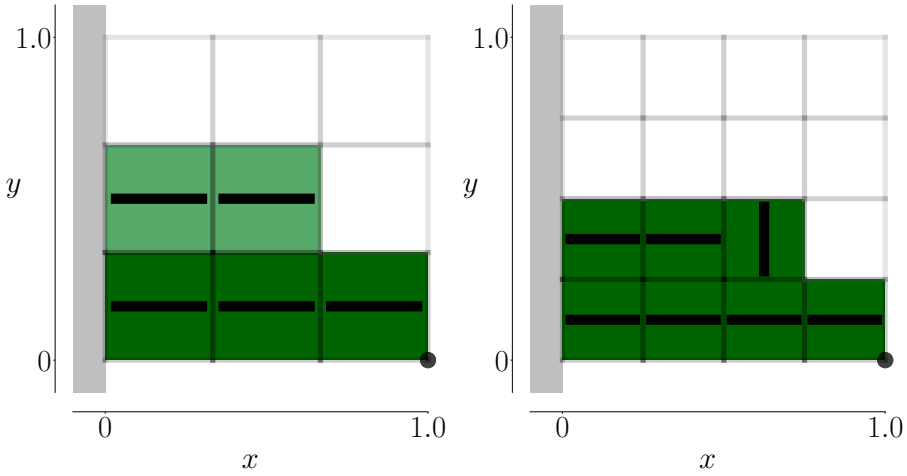

(a) 3×3 (b) 4×4

Fig. 7: Mass minimization result with discrete ply-angle and thickness variables (both problems are solved to global optimality). The light green indicates the thinner 0.03 m elements and the dark green indicates the thicker 0.1 m elements. The black lines show the ply orientation.

We use MOSEK to solve for the 4×4 case to global optimality and the result is shown in Figure 7b. A detailed convergence history is presented in Figure 9. About 0.0006% of total nodes have been explored in this case.

Table 5: Discrete ply-angle and discrete thickness mass minimization problem optimization time (sec) of different commercial solvers for 3×3 case

	Mixed integer optimization			Continuous relaxation		
	CPLEX	Gurobi	MOSEK	CPLEX	Gurobi	MOSEK
MISOCO–le	127.28	78.83	65.45	0.43	0.52	0.46
MISOCO–se	68.15	74.78	54.01	0.41	0.41	0.41
MISOCO–SOC-sparse	142.79	71.95	56.93	0.44	0.48	0.43
MISOCO–SOC-dense	230.11	61.64	54.26	0.60	0.51	0.49

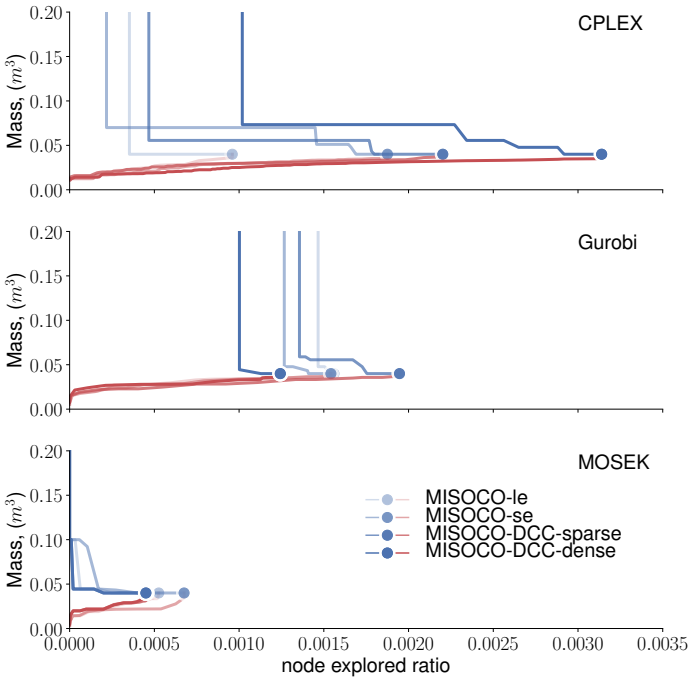

Fig. 8: Convergence history for different solvers using different formulations for the 3×3 discrete ply-angle and discrete thickness mass minimization problem. The x axis is the ratio of nodes explored versus the total node numbers which is equal to $(M+1)^N = 5^9$. The y axes represent the mass (in m^3 after dropping constant density). The red and blue curves are the lower and upper bounds, respectively. The blue dot indicates the point where optimality gap has been closed.

Table 6: Discrete ply-angle and discrete thickness mass minimization problem optimization time (sec) for the 4×4 case using MOSEK

	Mixed integer optimization	Continuous relaxation
MISOCO–se	51353.63	1.12

6.2 Stress-constrained compliance minimization problem

We consider a topology optimization problem where we minimize the compliance of a cantilevered plate subject to a tip load (Figure 10a and Figure 10b) with a mass constraint.

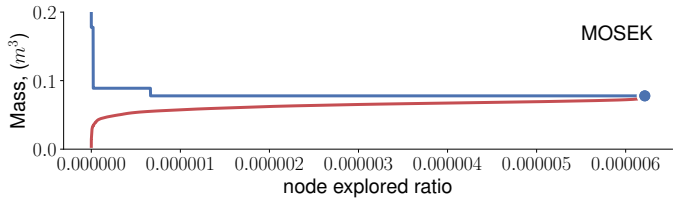

Fig. 9: Convergence history for MOSEK using MISOCO-se formulation for the 4×4 discrete ply-angle and discrete thickness mass minimization problem. The x axis is the ratio of nodes explored versus the total node numbers which is equal to $(M+1)^N = 5^{16}$. The y axis is the mass (in m^3 after dropping constant density). The red and blue curves are the lower and upper bounds, respectively. The blue dot indicates the point where optimality gap has been closed.

6.2.1 Discrete ply-angles only

The upper bound for mass is set to be $4/3$ times the corresponding mass optimization optimal mass. The design space for the ply angle is $\{0^\circ, 45^\circ, 90^\circ, 135^\circ\}$. The manufacturing constraints are enforced and the plate thickness is fixed to 0.1 m.

For the 3×3 cases, all solvers are able to find the optimal solution shown in Figure 10a. The computation times are listed in Table 7. Similarly to what we have observed in previous case, MOSEK solves the problem faster than the other two solvers. For MOSEK, the (MISOCO–le) and (MISOCO–SOC-Sparse) are faster than the other two formulations. Gurobi is faster than CPLEX for all cases. Similar with the previous mass minimization cases, the continuous relaxation solution time does not vary much among the solvers and formulations, except for the (MISOCO-SOC-dense) case. We show the convergence history in Figure 11. For all solvers solving all four formulations, less than 2.0% of total nodes have been explored before the optimality gap is closed. In general, CPLEX explores fewest nodes and thus is expected to give the fastest convergence. However, it is still the slowest among all three solvers. Therefore, the number of nodes explored is not consistent with the total solution time comparison for this case. However, we also notice that for MOSEK the numbers of nodes explored ranking is consistent with the total solution times ranking.

Table 7: Discrete ply-angle only compliance minimization problem optimization time (sec) of different solvers for the 3×3 case

	Mixed integer optimization			Continuous relaxation		
	CPLEX	Gurobi	MOSEK	CPLEX	Gurobi	MOSEK
MISOCO–le	908.06	614.23	252.37	0.43	0.52	0.46
MISOCO–se	704.15	492.62	385.40	0.41	0.41	0.41
MISOCO–SOC-sparse	851.25	528.46	240.35	0.44	0.48	0.43
MISOCO–SOC-dense	743.11	479.73	349.63	0.60	0.51	0.49

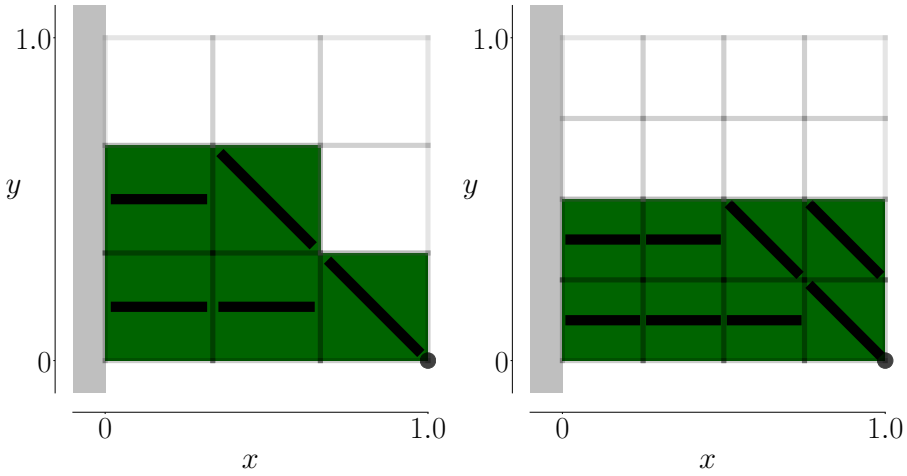

(a) 3×3 (b) 4×4

Fig. 10: Compliance minimization result with discrete ply-angle variables. The 3×3 case is solved to global optimality; while the 4×4 case is the best solution found in two days by MOSEK. The black lines indicate the ply orientation.

For the 4×4 case, the best result found by MOSEK within two days is shown in Figure 10b. A detailed convergence history is presented in Figure 12. However, the solver is not able to close the optimality gap in this case.

Table 8: Discrete ply-angle only compliance minimization problem optimization time (sec) for 4×4 case using MOSEK

	Mixed integer optimization time	Continuous relaxation solution time	lower bound	upper bound
MISOCO–se	172800	0.58	-1.260×10^3	1.667×10^2

6.2.2 Discrete ply-angle and discrete thickness variables

Similarly to the mass minimization section, in this section, we add discrete thickness as a design variable to our problem. The thickness could be either 0.1 m or 0.03 m. We restrict ourselves with $\{0^\circ, 90^\circ\}$ and drop the manufacturing constraint for this section for simplicity. The mass upper bound for mass is set to be $4/3\times$ the corresponding mass optimization optimal mass.

For the 3×3 case, the optimal solution is shown in Figure 13a and the solution times are listed in Table 9. In this case, CPLEX is the fastest for all formulations. For CPLEX, the (MISOCO–se) is faster than the other formulations. The lower bound

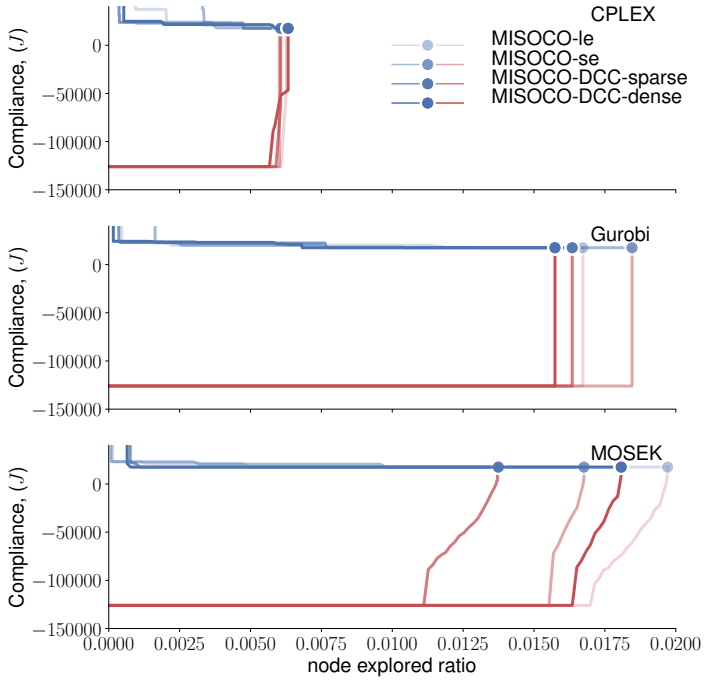

Fig. 11: Convergence history for different solvers using different formulations for the 3×3 discrete ply-angle only compliance minimization problem. The x axis is the ratio of nodes explored versus the total node numbers which is equal to $(M+1)^N = 5^9$. The y axes are the optimal compliances (in J). The red and blue curves are the lower and upper bounds, respectively. The blue dot indicates the point where optimality gap has been closed.

and the upper bound convergence history is shown in Figure 14. For all solvers solving all four formulations, fewer than 6.0% of total nodes have been explored before optimality gap being closed. For all formulations besides the (MISOCO-le) formulation, the number of nodes explored by CPLEX is lower than MOSEK, which in turn explores fewer nodes than Gurobi. This is consistent with their relative solution times.

For the 4×4 case, the best result found by MOSEK within two days is shown in Figure 13b. However, the solver is not able to close the optimality gap in this case within the 2-day time limit. A detailed convergence history is shown in Figure 15.

6.3 MISOCO augmented with a heuristic method

The optimizer solves a problem by collapsing an upper bound and a lower bound of a problem. The upper bound is given by a feasible solution and the lower bound is

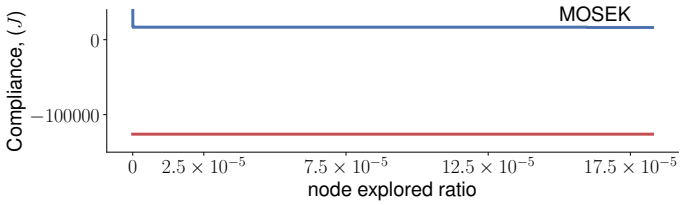

Fig. 12: Convergence history for MOSEK using MISOCO-se formulation for the 4×4 discrete ply-angle only compliance minimization problem. The x axis is the ratio of nodes explored versus the total node numbers which is equal to $(M+1)^N = 5^{16}$. The y axis is the compliances (in J). The red and blue curves are the lower and upper bounds, respectively. The optimality gap is still wide after the 2-day time limit.

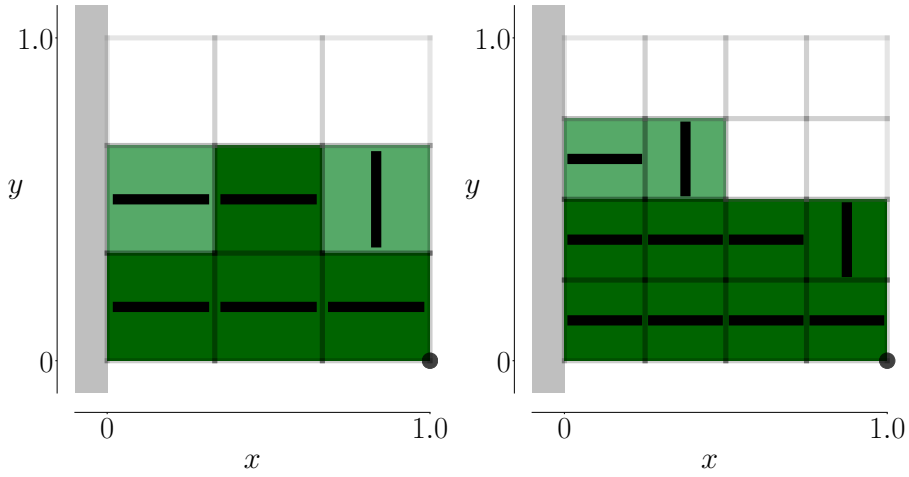

(a) 3×3 (b) 4×4

Fig. 13: Compliance minimization result with discrete ply-angle and thickness variables. The 3×3 case is solved to global optimality; while the 4×4 case is the best solution found in two days by MOSEK. The black lines indicate the ply orientation.

derived by solving continuous relaxation of the MISOCO subproblems in the B&B procedure. Here we consider the situation where SIMP and other methods are used to obtain a good initial guess but without a global optimality certificate and we want to give a global optimality certificate to the solution by solving MISOCO problems. We give the optimal solution previously found to represent a solution found by another strategy (e.g., GA) and investigate the computational time improvement. The results are listed in Tables 11 and 12. We use the Gurobi solver in this test due to its warm start capability.

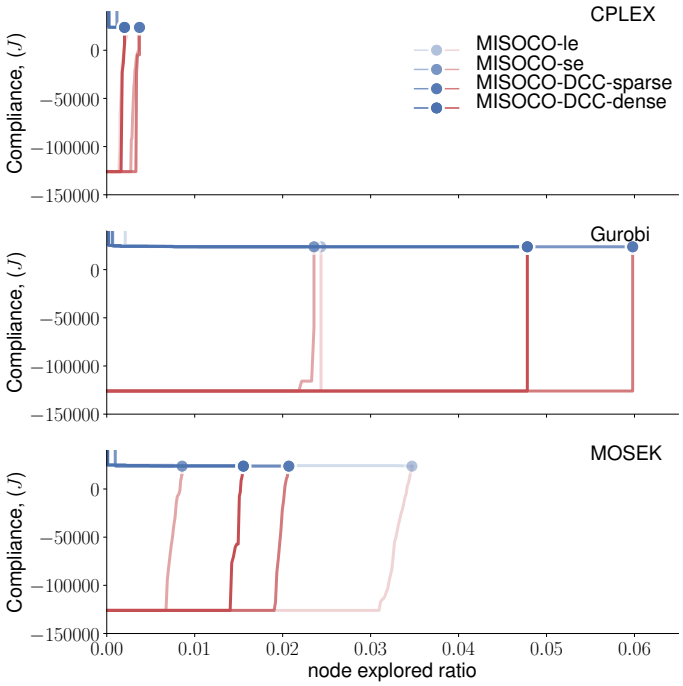

Fig. 14: Convergence history for different solvers using different formulations for the 3×3 discrete ply-angle and discrete thickness compliance minimization problem. The x axis is the ratio of nodes explored versus the total node numbers which is equal to $(M+1)^N = 5^9$. The y axes are the compliances (in J). The red and blue curves are the lower and upper bounds, respectively. The blue dot indicates the point where optimality gap has been closed.

Table 9: Discrete ply-angle and thickness compliance minimization problem optimization time (sec) of different commercial solvers for the 3×3 case

	Mixed integer optimization			Continuous relaxation		
	CPLEX	Gurobi	MOSEK	CPLEX	Gurobi	MOSEK
MISOCO–le	352.48	637.98	642.96	0.26	0.27	0.30
MISOCO–se	284.58	1075.11	385.88	0.29	0.30	0.33
MISOCO–SOC-sparse	375.89	1992.22	692.09	0.27	0.25	0.33
MISOCO–SOC-dense	362.68	830.17	712.45	0.19	0.28	0.32

For the mass warm start cases, the results are shown in Table 11. For all mass minimization cases with discrete angle as the only design variables, the optimization time is significantly reduced (for three out of four cases, it is more than 80%). If we consider both angle and thickness as design variable, (MISOCO–se) and (MISOCO–SOC-sparse) are improved, (MISOCO–SOC-dense) stay almost the same, but the

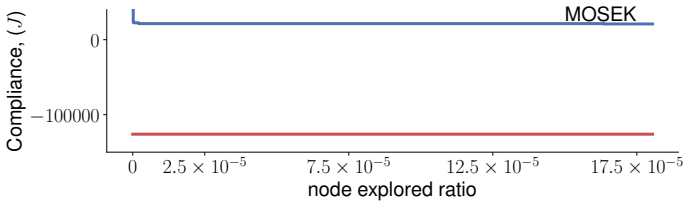

Fig. 15: Convergence history for MOSEK using MISOCO-se formulation for the 4×4 discrete ply-angle and discrete thickness compliance minimization problem. x axis is the ratio of nodes explored versus the total node numbers which is equal to $(M+1)^N = 5^{16}$. The y axis is the compliances (in J). The red and blue curves are the lower and upper bounds, respectively. The optimality gap is still wide after the 2-day time limit.

Table 10: Discrete ply-angle and thickness compliance minimization problem optimization time (sec) for 4×4 case using MOSEK

	Mixed integer optimization time	Continuous relaxation solution time	lower bound	upper bound
MISOCO–se	172800.0	0.59	-1.260×10^3	2.144×10^2

(MISOCO–le) is adversely affected. Over all, seven out of eight cases are improved, so it is beneficial to apply a warm start strategy to solve the mass minimization problem.

Table 11: Mass minimization problems with warm start for the Gurobi solver for the 3×3 cases

	Discrete ply-angle mass			Discrete ply-angle and thickness mass		
	Original	Warm start	Improvement	Original	Warm start	Improvement
MISOCO–le	313.20	45.22	85.6%	78.83	129.71	−64.5%
MISOCO–se	413.22	47.25	88.6%	74.78	28.08	62.4%
MISOCO–SOC-sparse	337.48	51.40	84.8%	71.95	56.89	20.9%
MISOCO–SOC-dense	151.86	61.45	59.5%	61.64	59.63	3.3%

The results for the compliance warm start cases are shown in Table 12. For all compliance minimization cases with discrete angle as the only design variables, the optimization time is negatively affected. If we consider both angle and thickness as the design variable, (MISOCO–se), (MISOCO–SOC-sparse) and (MISOCO–SOC-dense) are improved, but (MISOCO–le) is adversely affected. In general, the benefit of the warm start strategy for the compliance optimization problem is not clear. However, for the more challenging case where both ply-angle and thickness are design

variables, three out of four cases show significant improvement by using the warm start.

Table 12: Compliance minimization problems with warm start for the Gurobi solver for the 3×3 cases

	Discrete ply-angle compliance			Discrete ply-angle and thickness compliance		
	Original	Warm start	Improvement	Original	Warm start	Improvement
MISOCO–le	614.23	787.09	−28.1%	637.98	822.88	−29.0%
MISOCO–se	492.62	587.60	−19.3%	1075.11	452.18	57.9%
MISOCO–SOC-sparse	528.46	785.78	−48.7%	1992.22	431.77	78.3%
MISOCO–SOC-dense	479.73	598.46	−24.7%	830.17	459.91	44.6%

7 Conclusions

In this paper, we present various MISOCO formulations for the mass and compliance minimization of composite structures parametrized with discrete design variables. By using the state-of-the-art MISOCO solvers, we are able to solve the problems to global optimality. We compare the performances of four formulations of the Tsai–Wu failure criterion. Two out of four formulations are tightened using SOC constraints. There are several cases where the SOC tightened formulations yield the fastest results. However, in general there is no clear indication that one formulation is advantageous over another. We also compare the performances of different leading commercial MISOCO solvers: CPLEX, Gurobi, and MOSEK. We found that for our specific models, MOSEK usually outperforms the other two solvers. Finally, we explore a mixed solution strategy where the MISOCO solution time is improved by a warm start solution (possibly generated by another method like, SIMP type methods). This mixed solution strategy improved the solution time significantly for mass minimization problems in most cases. We demonstrated that the MISOCO strategy is capable to provide proven globally optimal structures for composite discrete ply-angle and thickness optimization problems. More research is needed to solve composite material optimization problems with significantly more elements and possibly with multiple layers.

8 Acknowledgments

This research was supported by Air Force Office of Scientific Research Grant No. FA9550-15-1-0222.

References

Achtziger W, Stolpe M (2007) Global optimization of truss topology with discrete bar areas—part II: Implementation and numerical results. Computational Optimization and Applications 44(2):315–341, DOI 10.1007/s10589-007-9152-7

Albanesi A, Bre F, Fachinotti V, Gebhardt C (2018) Simultaneous ply-order, ply-number and ply-drop optimization of laminate wind turbine blades using the inverse finite element method. Composite Structures 184:894–903, DOI 10.1016/j.compstruct.2017.10.051

Andersen ED, Andersen KD (2000) The MOSEK interior point optimizer for linear programming: An implementation of the homogeneous algorithm. In: Frenk H, Roos K, Terlaky T, Zhang S (eds) Applied Optimization, Springer US, pp 197–232, DOI 10.1007/978-1-4757-3216-0_8

Andersen ED, Roos K, Terlaky T (2003) On implementing a primal-dual interior-point method for conic quadratic optimization. Mathematical Programming 95(2):249–277, DOI 10.1007/s10107-002-0349-3

Belotti P, Góez JC, Pólik I, Ralphs TK, Terlaky T (2013) On families of quadratic surfaces having fixed intersections with two hyperplanes. Discrete Applied Mathematics 161(16-17):2778–2793, DOI 10.1016/j.dam.2013.05.017

Belotti P, Góez JC, Pólik I, Ralphs TK, Terlaky T (2017) A complete characterization of disjunctive conic cuts for mixed integer second order cone optimization. Discrete Optimization 24:3–31, DOI 10.1016/j.disopt.2016.10.001

Bendsøe MP, Sigmund O (1999) Material interpolation schemes in topology optimization. Archive of Applied Mechanics (Ingenieur Archiv) 69(9-10):635–654, DOI 10.1007/s004190050248

Bourdin B (2001) Filters in topology optimization. International Journal for Numerical Methods in Engineering 50(9):2143–2158, DOI 10.1002/nme.116

Brampton CJ, Wu KC, Kim HA (2015) New optimization method for steered fiber composites using the level set method. Structural and Multidisciplinary Optimization 52(3):493–505, DOI 10.1007/s00158-015-1256-6

Brooks TR, Martins JRRA (2018) On manufacturing constraints for tow-steered composite design optimization. Composite Structures 204:548–559, DOI 10.1016/j.compstruct.2018.07.100

Bruyneel M (2010) SFP—a new parameterization based on shape functions for optimal material selection: Application to conventional composite plies. Structural and Multidisciplinary Optimization 43(1):17–27, DOI 10.1007/s00158-010-0548-0

Cheng G (1995) Some aspects of truss topology optimization. Structural Optimization 10(3-4):173–179, DOI 10.1007/bf01742589

Cheng GD, Guo X (1997) ε-relaxed approach in structural topology optimization. Structural Optimization 13(4):258–266, DOI 10.1007/bf01197454

Diaz A, Sigmund O (1995) Checkerboard patterns in layout optimization. Structural Optimization 10:40–45

Ghiasi H, Fayazbakhsh K, Pasini D, Lessard L (2010) Optimum stacking sequence design of composite materials part II: Variable stiffness design. Composite Structures 93(1):1–13, DOI 10.1016/j.compstruct.2010.06.001

Gillet A, Francescato P, Saffre P (2009) Single- and multi-objective optimization of composite structures: The influence of design variables. Journal of Composite Materials 44(4):457–480, DOI 10.1177/0021998309344931

Grossmann IE, Voudouris V, Ghattas O (1992) Mixed-integer linear programming reformulations for some nonlinear discrete design optimization problems. In: Floudas CA, Pardalos PM (eds) Recent advances in global optimization, Princeton University Press, pp 478–512

Gurobi Optimization, LLC (2018) Gurobi optimizer reference manual. URL `http://www.gurobi.com`

Haftka RT (1985) Simultaneous analysis and design. AIAA Journal 23(7):1099–1103, DOI 10.2514/3.9043

Haftka RT, Walsh JL (1992) Stacking-sequence optimization for buckling of laminated plates by integer programming. AIAA Journal 30(3):814–819, DOI 10.2514/3.10989

Hahn HT, Tsai SW (1980) Introduction to Composite Materials. Technomic Publishing Co, Inc.

Huang D, Friedmann PP (2016) An integrated aerothermoelastic analysis framework for predicting the response of composite panels. In: 15th Dynamics Specialists Conference, American Institute of Aeronautics and Astronautics, DOI 10.2514/6.2016-1090

IBM ILOG (2018) IBM ILOG CPLEX v12.8.0 user's manual for CPLEX. URL `http://www.cplex.com`

Kennedy GJ (2016) A full-space barrier method for stress-constrained discrete material design optimization. Structural and Multidisciplinary Optimization 54(3):619–639, DOI 10.1007/s00158-016-1428-z

Kennedy GJ, Martins JRRA (2013) A laminate parametrization technique for discrete ply angle problems with manufacturing constraints. Structural and Multidisciplinary Optimization 48(2):379–393, DOI 10.1007/s00158-013-0906-9

Kim JS, Kim CG, Hong CS (1999) Optimum design of composite structures with ply drop using genetic algorithm and expert system shell. Composite Structures 46(2):171–187, DOI 10.1016/s0263-8223(99)00052-5

Marmaras K (2014) Optimal design of composite structures under manufacturing constraints. PhD thesis, Technical University of Denmark

Martins JRRA, Lambe AB (2013) Multidisciplinary design optimization: A survey of architectures. AIAA Journal 51(9):2049–2075, DOI 10.2514/1.J051895

Mela K (2014) Resolving issues with member buckling in truss topology optimization using a mixed variable approach. Structural and Multidisciplinary Optimization 50(6):1037–1049, DOI 10.1007/s00158-014-1095-x

Munoz E (2010) Global optimization for discrete topology design problems by generalized Benders's decomposition. PhD thesis, Technical University of Denmark

Nikbakt S, Kamarian S, Shakeri M (2018) A review on optimization of composite structures part i: Laminated composites. Composite Structures 195:158–185, DOI 10.1016/j.compstruct.2018.03.063

Petersen CC (1971) A note on transforming the product of variables to linear form in linear programs. Working Paper, Purdue University,

Rasmussen M, Stolpe M (2008) Global optimization of discrete truss topology design problems using a parallel cut-and-branch method. Computers & Structures 86(13-14):1527–1538, DOI 10.1016/j.compstruc.2007.05.019

Riche RL, Haftka RT (1993) Optimization of laminate stacking sequence for buckling load maximization by genetic algorithm. AIAA Journal 31(5):951–956, DOI 10.2514/3.11710

Shahabsafa M (2018) Mixed integer conic optimization and its applications. PhD thesis, Lehigh University

Shahabsafa M, Mohammad-Nezhad A, Terlaky T, Zuluaga L, He S, Hwang JT, Martins JRRA (2018) A novel approach to discrete truss design problems using mixed integer neighborhood search. Structural and Multidisciplinary Optimization 58:2411—2429, DOI 10.1007/s00158-018-2099-8

Sigmund O (1994) Design of material structures using topology optimization. PhD thesis, Technical University of Denmark

Sigmund O (1998) Numerical instablities in topology optimization: A survey on procedures dealing with checkerboards, mesh-dependencies and local minima. Structural Optimization 16:68–75

Sørensen R, Lund E (2015) Thickness filters for gradient based multi-material and thickness optimization of laminated composite structures. Structural and Multidisciplinary Optimization 52(2):227–250, DOI 10.1007/s00158-015-1230-3

Sørensen SN, Stolpe M (2015) Global blending optimization of laminated composites with discrete material candidate selection and thickness variation. Structural and Multidisciplinary Optimization 52(1):137–155, DOI 10.1007/s00158-015-1225-0

Stegmann J, Lund E (2005) Discrete material optimization of general composite shell structures. International Journal for Numerical Methods in Engineering pp 2009–2027, DOI 10.1002/nme.1259, URL http://dx.doi.org/10.1002/nme.1259

Stolpe M (2007) On the reformulation of topology optimization problems as linear or convex quadratic mixed 0–1 programs. Optimization and Engineering 8(2):163–192, DOI 10.1007/s11081-007-9005-3

Stolpe M (2014) Truss topology optimization with discrete design variables by outer approximation. Journal of Global Optimization 61(1):139–163, DOI 10.1007/s10898-014-0142-x

Stolpe M, Stidsen T (2007) A hierarchical method for discrete structural topology design problems with local stress and displacement constraints. International Journal for Numerical Methods in Engineering 69(5):1060–1084, DOI 10.1002/nme.1800

Stolpe M, Svanberg K (2003) Modelling topology optimization problems as linear mixed 0-1 programs. International Journal for Numerical Methods in Engineering 57(5):723–739, DOI 10.1002/nme.700

Sved G, Ginos Z (1968) Structural optimization under multiple loading. International Journal of Mechanical Sciences 10(10):803–805, DOI 10.1016/0020-7403(68)90021-0

Tsai SW, Wu EM (1971) A general theory of strength for anisotropic materials. Journal of composite materials 5(1):58–80

Zhou Y, Nomura T, Saitou K (2018) Multi-component topology and material orientation design of composite structures (MTO-c). Computer Methods in Applied Mechanics and Engineering 342:438–457, DOI 10.1016/j.cma.2018.07.039

Appendix

1. Constitutive matrix calculation

1.a In-plane constitutive relation

In this section, we present the constitutive matrix $\mathbf{Q}_i$ derivation procedures. In a frame that the x axis is aligned with the fiber direction, we have the following constitutive relationships:

$$\begin{bmatrix} \sigma_1 \\ \sigma_2 \\ \tau_{12} \end{bmatrix} \mathbf{Q} \begin{bmatrix} \varepsilon_1 \\ \varepsilon_2 \\ \varepsilon_{12} \end{bmatrix},$$

where $\mathbf{Q}$ is given as

$$\mathbf{Q} = \begin{bmatrix} Q_{11} & Q_{12} & 0 \\ Q_{21} & Q_{22} & 0 \\ 0 & 0 & 2Q_{66} \end{bmatrix},$$

and

$$\begin{aligned} Q_{11} &= \frac{E_1}{1-\nu_{21}\nu_{12}} \\ Q_{12} &= \frac{\nu_{12}E_2}{1-\nu_{21}\nu_{12}} = Q_{21} \\ Q_{22} &= \frac{E_2}{1-\nu_{21}\nu_{12}} \\ Q_{66} &= G_{12}. \end{aligned}$$

For more general cases where the x axis and the fiber direction are with an angle of θ, using the laws of tensor transformation relations, we have:

$$\begin{bmatrix} \sigma_x \\ \sigma_y \\ \tau_{xy} \end{bmatrix} = \mathbf{T}^{-1}(\theta) \begin{bmatrix} \sigma_1 \\ \sigma_2 \\ \tau_{12} \end{bmatrix},$$

where

$$\mathbf{T}^{-1}(\theta) = \begin{bmatrix} \cos^2\theta & \sin^2\theta & -2\cos\theta\sin\theta \\ \sin^2\theta & \cos^2\theta & 2\cos\theta\sin\theta \\ \cos\theta\sin\theta & -\cos\theta\sin\theta & \cos^2\theta-\sin^2\theta \end{bmatrix},$$

and

$$\begin{bmatrix} \varepsilon_1 \\ \varepsilon_2 \\ \varepsilon_{12} \end{bmatrix} = \mathbf{T}(\theta) \begin{bmatrix} \varepsilon_x \\ \varepsilon_y \\ \varepsilon_{xy} \end{bmatrix}.$$

Thus, the general constitutive law is given as:

$$\begin{bmatrix} \sigma_x \\ \sigma_y \\ \tau_{xy} \end{bmatrix} = \mathbf{T}^{-1}(\theta)\mathbf{Q}\mathbf{T}(\theta) \begin{bmatrix} \varepsilon_x \\ \varepsilon_y \\ \varepsilon_{xy} \end{bmatrix}.$$

For the j^{th} choice with the angle as θ_j, we define:

$$\mathbf{Q}_j = \mathbf{T}^{-1}(\theta_j)\mathbf{Q}\mathbf{T}(\theta_j).$$

We can give an explicit expression for $\mathbf{Q}_j$ by expanding the previous equation:

$$\begin{aligned}
Q_{j,11} &= Q_{11}\cos^4\theta_j + Q_{22}\sin^4\theta_j + 2(Q_{12}+2Q_{66})\sin^2\theta_j\cos^2\theta_j \\
Q_{j,12} &= (Q_{11}+Q_{22}-4Q_{66})\cos^2\theta_j\sin^2\theta_j + Q_{12}(\sin^4\theta_j+\cos^4\theta_j) \\
Q_{j,22} &= Q_{11}\sin^4\theta_j + Q_{22}\cos^4\theta_j + 2(Q_{12}+2Q_{66})\sin^2\theta_j\cos^2\theta_j \\
Q_{j,16} &= (Q_{11}-Q_{12}-2Q_{66})\cos^3\theta_j\sin\theta_j - (Q_{22}-Q_{12}-2Q_{66})\cos\theta_j\sin^3\theta_j \\
Q_{j,26} &= (Q_{11}-Q_{12}-2Q_{66})\cos\theta_j\sin^3\theta_j - (Q_{22}-Q_{12}-2Q_{66})\cos^3\theta_j\sin\theta_j \\
Q_{j,66} &= (Q_{11}+Q_{22}-2Q_{12}-2Q_{66})\cos^2\theta_j\sin^2\theta_j + Q_{66}(\sin^4\theta_j+\cos^4\theta_j).
\end{aligned}$$

1.b Out-of-plane constitutive relation

The out-of-plane constitutive relationship is given as

$$\begin{bmatrix}\sigma_{yz}\\ \sigma_{xz}\end{bmatrix} = \mathbf{C}_j \begin{bmatrix}\psi_y + \frac{\partial w}{\partial y}\\ \psi_x + \frac{\partial w}{\partial x},\end{bmatrix},$$

where

$$\mathbf{C}_j = \begin{bmatrix}C_{j,44} & C_{j,45}\\ C_{j,45} & C_{j,55}\end{bmatrix},$$

and

$$\begin{aligned}
C_{j,44} &= C_{44}\cos^2\theta_j + C_{55}\sin^2\theta_j \\
C_{j,45} &= (C_{55}-C_{44})\cos\theta_j\sin\theta_j \\
C_{j,55} &= C_{44}\sin^2\theta_j + C_{55}\cos^2\theta_j.
\end{aligned}$$

We also know that $C_{44} = G_{23}$ and $C_{55} = G_{12}$.

2. Strain operator

We calculate the strain at the upper surface center for each element that is later used in Tsai–Wu failure criterion. The in-plane strain is given as:

$$\varepsilon = \varepsilon_l + z\chi, \varepsilon_l = \mathbf{L}_1\mathbf{u}, \chi = \mathbf{L}_2\mathbf{u},$$

where

$$\mathbf{L}_1 = \left[\begin{array}{c|ccccc|c} \cdots & N_{i,x} & 0 & 0 & 0 & 0 & \cdots \\ & 0 & N_{i,y} & 0 & 0 & 0 & \\ & N_{i,y} & N_{i,x} & 0 & 0 & 0 & \end{array}\right], \mathbf{L}_2 = \left[\begin{array}{c|ccccc|c} \cdots & 0 & 0 & 0 & N_{i,x} & 0 & \cdots \\ & 0 & 0 & 0 & 0 & N_{i,y} & \\ & 0 & 0 & 0 & N_{i,y} & N_{i,x} & \end{array}\right].$$

For the shape function N_i, we have

$$\begin{aligned} N_{i+3j-3} &= f_i(\eta) f_j(\xi), ij = 1,2,3 \\ f_1(x) &= \frac{1}{2}x(x-1) \\ f_2(x) &= 1-x^2 \\ f_3(x) &= \frac{1}{2}(1+x)x. \end{aligned}$$

To evaluate the strain at the center point over the top surface, we simply set $(\eta, \xi, z) = (0,0,h/2)$. Finally,

$$\varepsilon_i^l = \mathbf{B}(\mathbf{x}_i^l)\mathbf{u}_i = \left(\mathbf{L}_1(0) + \frac{h}{2}\mathbf{L}_2(0)\right)\mathbf{u}_i.$$

3. Local stiffness matrix calculation

In this section, we present the derivation of the local stiffness matrix $\mathbf{K}_{ij}$ derivation, which is based on classic lamination theory (CLT). We begin the derivation by giving the expression for matrices $\mathbf{A}, \mathbf{B}, \mathbf{D}$ representing the extensional stiffness matrix, the coupling stiffness matrix and the bending stiffness matrix, respectively:

$$\left[\mathbf{A}\ \mathbf{B}\ \mathbf{D}\right] = \int_{-h_i/2}^{h_i/2} \left[1\ z\ z^2\right] \mathbf{Q}_j dz.$$

The traverse shear stiffness matrix is given as:

$$\mathbf{S} = \kappa \int_{-h/2}^{h/2} \mathbf{C}_j,$$

where $\kappa = \frac{5}{6}$. Notice that to be consistent with the assumption made in this paper here we assume that there is only one layer of material.

We now present the stiffness matrix expression:

$$\begin{aligned} \mathbf{K}_{ij} &= \mathbf{K}_{ij,L_1} + \mathbf{K}_{ij,L_2} \\ &= \int_{A_i} \left(L_1^\intercal \mathbf{A} L_1 + L_1^\intercal \mathbf{B} L_2 + L_2^\intercal \mathbf{B} L_1 + L_2^\intercal \mathbf{D} L_2\right) dA_i + \int_{A_i} \left(L_3^\intercal \mathbf{S} L_3\right) dA_i \end{aligned}$$

Then we apply the Gaussian quadrature for numerical integration. For K_{ij,L_1}, we apply 3×3 integration points; while for K_{ij,L_2}, we apply 2×2 integration points. This helps to avoid "shear locking".